



# Kinetic analysis of p-rGO/n-TiO<sub>2</sub> nanocomposite generated by hydrothermal technique for simultaneous photocatalytic water splitting and degradation of methylene blue dye

Hager M. Moustafa<sup>1</sup> · Mohamed S. Mahmoud<sup>1,2</sup> · Mamdouh M. Nassar<sup>1</sup>

Received: 7 June 2022 / Accepted: 29 September 2022 / Published online: 7 October 2022  
© The Author(s), under exclusive licence to Springer-Verlag GmbH Germany, part of Springer Nature 2022

## Abstract

In this study, the nanocomposites of reduced graphene oxide/TiO<sub>2</sub> (rGO/TiO<sub>2</sub> with different percentages) have been synthesized using a modified Hummers' method followed by hydrothermal treatment. The morphology and bonding structure of the prepared samples have been characterized by Fourier-transform infrared spectroscopy (FTIR), transmission electron microscopy (TEM), scanning electron microscopy (SEM), X-ray diffractometry (XRD), and X-ray photoelectron spectroscopy (XPS). The photo-characteristic aspects of the prepared samples have been indicated by photoluminescence (PL) emission spectroscopy and ultraviolet-visible diffuse reflection spectroscopy (DRS). The photocatalytic performance of rGO/TiO<sub>2</sub> demonstrated that it is an effective photocatalyst for methylene blue (MB) dye decomposition through illumination by a mercury lamp. Within 60 min of continuous irradiation, the nanocomposite-induced MB decomposition reached a rate of over 99%. Different MB concentrations and optimal percent loadings in catalysts have been investigated. Furthermore, the results showed that as the amount of catalyst increased, the decomposition of MB enhanced. Finally, the loading percentage of rGO with TiO<sub>2</sub> has been studied, and an empirical equation relating the reaction rate constant until the mass of the photocatalyst and dye concentration has been proposed. The results showed that the prepared nanocomposites had good photocatalytic activity toward water splitting and photo-decomposition of MB.

**Keywords** Nanocomposite catalyst · Photocatalytic degradation · Hydrothermal treatment · Hydrogen generation

## Introduction

Environmental pollution and the global energy problem were currently major concerns of all countries. The United Nations has already set the 17 global Sustainable Development Goals (SDGs). One of these goals is to provide universal and equitable access to safe and affordable drinking water for all by 2030. However, statistics show that there has been slow advancement toward achieving this goal in most countries (Raghavalu Thirumalai et al. 2013). Consequently, it was crucial to investigate more about more

sustainable ways for wastewater treatment to alleviate the potential risk of wastewater disposal without proper treatment. Therefore, innovative wastewater treatment methods were prominent factors for the achievement of sustainable wastewater provision (Teodosiu and Fiore 2019). Renewable-based wastewater treatment could help many countries achieve some of the SDGs as it utilizes a clean energy source to clean wastewater with a lower carbon footprint. Among the renewable-based processes, photocatalytic decomposition of organic matter was a promising one that could break down organic contaminants efficiently (Li et al. 2017). Water contamination involves the presence of several contaminants like highly poisonous heavy metals (i.e., chromium (Cr), iron (Fe), manganese (Mn), lead (Pb)) and organic pollutants such as MB, methyl orange (MO), rhodamine, and phenols. When the organic contaminants react with air and water, toxic end products could result. Consequently, it was essential to breakdown the organic pollutants efficiently (Ahmad et al. 2013; Li et al. 2016a; Jahanara and Farhadi 2019; Tao et al. 2019; Ramar and Balasubramanian 2021). The ability

Responsible Editor: Sami Rtimi

✉ Mohamed S. Mahmoud  
m.salah.m@mu.edu.eg

<sup>1</sup> Chemical Engineering Department, Minia University, El-Minia 61516, Egypt

<sup>2</sup> Department of Engineering, University of Technology and Applied Sciences, Suhar 311, Sultanate of Oman

of the semiconductor to effectively absorb light and form electron–hole pairs that can stimulate dye decomposition reactions affects the photocatalytic activity for dye decomposition. The MB was an intensely colored compound that was used in dyeing and printing textiles and was a common water pollutant (Rauf et al. 2010; Pradhan et al. 2013; Benjwal et al. 2015; Meenakshisundaram 2017; Al-Mamun et al. 2019; Nazari and Salem 2019; Gopinath et al. 2020; Khan et al. 2022). The most recent research effort to improve green energy generation systems and sustainable pollution management techniques took several paths, including photocatalytic processes. The demand for energy and the emission of hazardous waste materials into the environment are increasing as the human population and industrial growth accelerate. Photon-induced water splitting in the presence of photocatalysts was a sustainable way to overcome the intermittent issues of solar power utilization and provide a green alternative to fossil fuels (Deb Nath et al. 2019; Buliyaminu et al. 2020; Mahfoz et al. 2020; Ullah et al. 2020). Production of hydrogen utilizing suitable photocatalyst and solar energy was significant not only because it was an effective way to produce large-scale renewable and clean hydrogen, but also because it helped to avoid potential energy-storage difficulties. Photocatalytic water splitting was one of the most practical approaches in this area (Qi et al. 2019; Shah et al. 2019; Wang et al. 2019; Timmerberg et al. 2020; Yaqoob et al. 2020). Recent research on a green and sustainable water splitting process using heterogeneous semiconductor photocatalysts that simulate natural photosynthesis has received a lot of interest as a way to solve energy problems and environmental issues (Acharya et al. 2020; Iervolino et al. 2020; Nayak and Parida 2020; Nayak and Parida 2021).

Due to the manufacture of a wide range of products, environmental pollutant reduction, and production of clean energy ( $H_2$  and  $O_2$ ), semiconductor photocatalysts have attracted additional research interest (Yan et al. 2020; Boumeriame et al. 2021; Kranz and Wächter 2021; Liu et al. 2021). Over the last 40 years, titanium dioxide ( $TiO_2$ ), a promising semiconductor with high chemical stability, remarkable oxidizing activity, nontoxicity, and photo-corrosion resistance, has played a key role in the advancement of semiconductor photocatalysis in the field of PEC hydrogen production (Li et al. 2020; Peiris et al. 2021). Because of its increased redox potential and strong photocatalytic activity,  $TiO_2$  is an effective semiconductor material that is currently being investigated and widely used in significant photo-catalytic reactions (Singh and Dutta 2018; Guo et al. 2019; Reddy et al. 2020; Zhao et al. 2020; Sonu et al. 2021).

Enormous research efforts have been made to improve the utilization of  $TiO_2$  as a photocatalyst by using dopants, modifying the surface, and depositing noble metals. However, these single photocatalysts had drawbacks such as

limited photocatalytic hydrogen production activity, low stability, and high cost. A nanocomposite should have excellent carrier mobility, good charge separation, a longer carrier lifetime, and good light absorption to qualify as an effective photocatalyst (Lim et al. 2019; Eidsvåg et al. 2021; Hajjalilou et al. 2021). Some of these properties are not found in widely used single and mixed metal oxides and metal sulfides. By introducing noble metals or rGO, these limits could be overcome. This was because of its unique structure, good electrical properties, sustainable qualities, high carrier mobility, as well as its chemical stability, and cost-effectiveness (Morales-Torres et al. 2012; Kumar et al. 2018; Liu et al. 2018; Shang et al. 2018; Zhang et al. 2020; Mondal et al. 2021).

Graphene is the basic structure of all other carbon allotropes (Mohan et al. 2018; Yu et al. 2018). Several papers have already been published in this field on the synthesis, modification, and application of graphene-based photocatalysts for energy and environmental solutions, such as graphene doping, graphene in photocatalysis, graphene and graphene oxide sponge, functional modification of graphene/graphene oxide, nitrogen-doped graphene, graphene nanocomposite mechanics, and graphene strain engineering (Li et al. 2016b; Ribao et al. 2017; Soltani et al. 2018; Yang et al. 2018; Singh et al. 2020a; Yu et al. 2020; Usman et al. 2021; Purabgola et al. 2022). Although there are many functions of the co-catalysts in the photocatalytic reactions, their main role is to postpone the  $e/h$  recombination rate. In the case of rGO, the retardation of recombination is attained by moving the electrons to the co-catalyst. This happens because of the presence of a lower Fermi level than  $TiO_2$ . The presence of the co-catalysts improves the  $H_2$  production step by stimulating an extra step of the water-splitting process, namely by reducing the activation barrier of the surface reactions. Purabgola et al. indicated that the presence of the co-catalysts doped with the  $TiO_2$  nanoparticles can reduce the band gap and thus expand the activity of the photocatalyst through the visible light region (Purabgola et al. 2022). Usually, the hydrogen evolution reaction is triggered by the presence of extra electrons in the conduction band of the photocatalyst. Hence, removal of the photo-generated holes on the valence band of the photocatalyst surface is required to speed up the hydrogen production reaction. Typically, these holes are removed by the sluggish oxygen evolution reaction, but due to the different speeds of hydrogen and oxygen evolution reactions, it is necessary to move part of the holes to the electrolyte by the addition of certain hole scavenger ions in the reaction solution. Various types of hole scavengers have been reported, including alcohols; methanol (Bamwenda and Arakawa 2001; Chen et al. 2010; Zhang et al. 2014; Kim et al. 2016; Tran et al. 2017); inorganic ions like  $S^{2-}$ ,  $SO_3^{2-}$ ,  $H_2S$ ,  $I^-/IO_3^-$ , and

$\text{Fe}^{2+}$  (Badawy et al. 2011; Kim et al. 2014; Wang et al. 2017; Bharatvaj et al. 2018); and organic acids (Koca and Şahin 2002; Zhang et al. 2013).

The mechanism of hole scavenger is to transfer the holes, accompanied by decomposition of the organic molecules or changing the valence state of the ions. Nevertheless, the presence of the scavengers seems to increase the overall hydrogen production cost. Also, some organic scavengers are toxic, which will exhibit bad effect in the long run. Alternatively, the organic matter naturally available in the wastewater could act as a free source scavenger for hydrogen production reactions. Therefore, if the holes can react with the naturally available organic pollutants, the *e/h* recombination rate can be inhibited and the hydrogen production rate will be improved (Wu et al. 2022). Although  $\text{TiO}_2$  has thermodynamically suitable energy band positions to decompose organic matters, it suffers from poor visible light absorption and weak surface interaction with organic matters (Naldoni et al. 2019). Therefore, the presence of oxygen vacancies (OVs) has been intensively studied to overcome the poor visible light absorption. These OVs can induce the decomposition reaction of  $\text{H}_2\text{O}$  to produce active hydroxyl groups, which in turn is converted to hydroxyl radicals ( $\text{OH}^*$ ) that can decompose organic pollutants efficiently. Accordingly, using a photocatalyst for dual hydrogen production and wastewater treatment would provide double goals of energy reduction and wastewater treatment (Cheng et al. 2012; Gao et al. 2012; Mino et al. 2016; Hafeez et al. 2018; Asgharza-deh and Eslami 2019).

In this study, a photocatalyst (rGO/ $\text{TiO}_2$  nanocomposites) has been synthesized by doping rGO with  $\text{TiO}_2$  nanoparticles. The nanocomposites are being used to investigate the effect of photocatalytic efficiency on both hydrogen production and photocatalytic decomposition of MB, a possible mechanism for removing MB under a mercury lamp. Moreover, the decomposition of MB dye as a water pollutant model is used to evaluate the photocatalytic activity of the produced nanocomposites where MB is a photoactive phenothiazine dye. The results confirm that the rGO/ $\text{TiO}_2$  nanocomposite has the potential to be a versatile photocatalyst

for the production of hydrogen and the photodecomposition of organic dyes in industrial effluent.

## Experimental procedure

### Materials

All chemicals have been purchased and used without further purification. Graphite powder, potassium permanganate ( $\text{KMnO}_4$ ), MB, and titanium isopropoxide were obtained from Sigma-Aldrich chemicals. Sulfuric acid ( $\text{H}_2\text{SO}_4$ , 98%, Scharlau), hydrochloric acid (HCl 35–38%, Loba Chemie), ortho-phosphoric acid ( $\text{H}_3\text{PO}_4$ , 85%, Germany), and hydrogen peroxide ( $\text{H}_2\text{O}_2$  30%, EL Naser Ph. ADWIC) were procured from Finar Chemicals Limited.

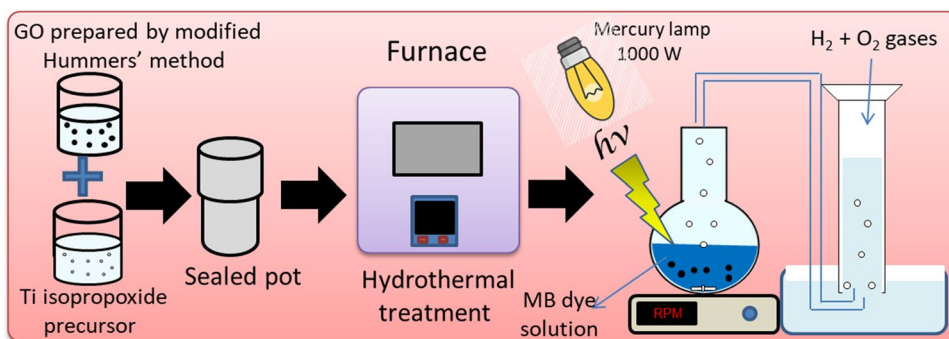
### Synthesis of graphene oxide (GO)

Figure 1 shows a schematic representation of the setup and procedures. The modified Hummers' method is used to make graphene oxide (Hummers Jr and Offeman 1958). The procedure for GO preparation using the modified Hummers' method is explained in previous work (Moustafa et al. 2020).

### Synthesis of rGO– $\text{TiO}_2$ binary heterostructure photocatalysts

The hydrothermal technique is used to synthesize the binary heterostructured photocatalyst reduced graphene oxide rGO/ $\text{TiO}_2$ . To enhance material exfoliation, GO were suspended in ethanol for 1 h. The exfoliated GO were then re-exfoliated in an ethanol solution using ultra sonication for 2 h. To produce a homogenous dispersion of the materials, an aqueous solution of re-exfoliated GO mixed with  $\text{TiO}_2$  was agitated slowly before hydrothermal treatment at 300 °C for 4 h (Singh et al. 2020a).

**Fig. 1** Schematic representation of the setup and procedures



## Photocatalytic water splitting procedure

The photocatalytic H<sub>2</sub> production studies were carried out in a 250-mL conical flask with two openings, one of which is sealed with silicone rubber and the other is connected by a rubber hose to an inclined graduated cylinder. This cylinder is filled with water and is inserted upside down into a beaker to determine the volume of the gas that will displace the water. A mercury lamp (2000 W) is employed as a light source. It is placed about 20 cm from the photocatalytic reactor. For the photon-induced water splitting experiment, 0.2 g of powder photocatalysts are suspended in 100 mL of an aqueous solution containing 50 ppm MB solution. To enhance the mass transfer of the reaction and prevent particles from settling at the bottom of the reactor, the suspension is maintained in mixing with a magnetic stirrer.

## Photocatalytic decomposition of MB dye

Under a mercury lamp, the photocatalytic activity of the as-synthesized rGO/TiO<sub>2</sub> nanocomposite is evaluated for the decomposition of MB at a wavelength of 365 nm. The same setup for hydrogen production is employed, except the concentration of the MB is the parameter to be investigated. The photocatalytic activity of the nanocomposite is determined by observing the photodecomposition of MB at various catalyst loadings ranging from 5 to 50 mg/L. This nanocomposite is suspended in a solution containing different concentrations of MB dye (5 to 200 ppm). Also, the suspension is agitated at 300 rpm to facilitate the photocatalytic decomposition. The absorption spectra of the supernatant were measured using a Shimadzu UV-1800 spectrophotometer to monitor the change in the dye concentration. During the experiment, a 5 mL sample of the suspension is taken every 10 min, centrifuged for 5 min at 14,000 rpm, tested using a spectrophotometer, and returned back to the flask.

## Characterization

A typical characterization of nanoparticles has been employed in this study. Fourier transform infrared (FTIR) spectroscopy has been utilized to estimate the different chemical bonds in the nanocomposite sample. It is in the range of 4000 to 500 cm<sup>-1</sup> using a Nicolet Avatar 370 spectrometer. The surface of the nanocomposite samples and morphology are also identified by transmission electron microscopy (TEM) analysis (JEOL-100CXII microscope with an accelerating voltage of 200 kV) and scanning electron microscopy (SEM/EDX) (Hitachi S-4800 field emission SEM with a voltage of 10 kV). XPS analysis (K-ALPHA, Thermo Fisher Scientific, USA) with monochromatic X-ray Al K-radiation –10 to 1350 eV and a spot size of 400 nm at

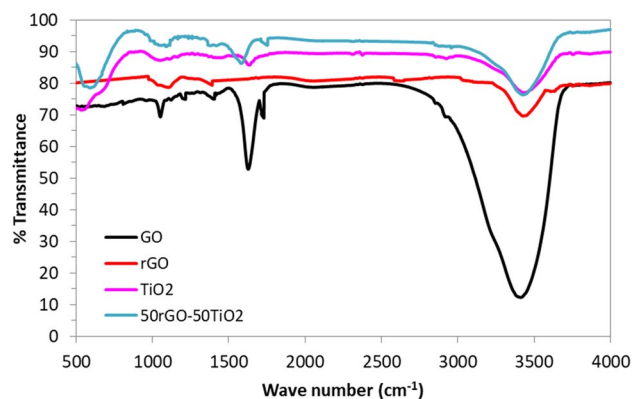
a pressure of 10<sup>-9</sup> bar is used to reveal the presence of Ti, O, and C elements. Also, XRD experiment is carried out with (Bruker D8 diffractometer using Cu K $\alpha$  radiation at 40 kV and 40 mA;  $\lambda = 1.5406 \text{ \AA}$ ). The FLS920 full-function steady-state/transient fluorescence spectrometer is used to characterize the photoluminescence (PL) spectra. On a Jasco V-770, diffuse reflectance spectra (DRS) are acquired using barium sulfate as a reference.

## Results and discussion

### Characterization of the nanocomposite photocatalyst

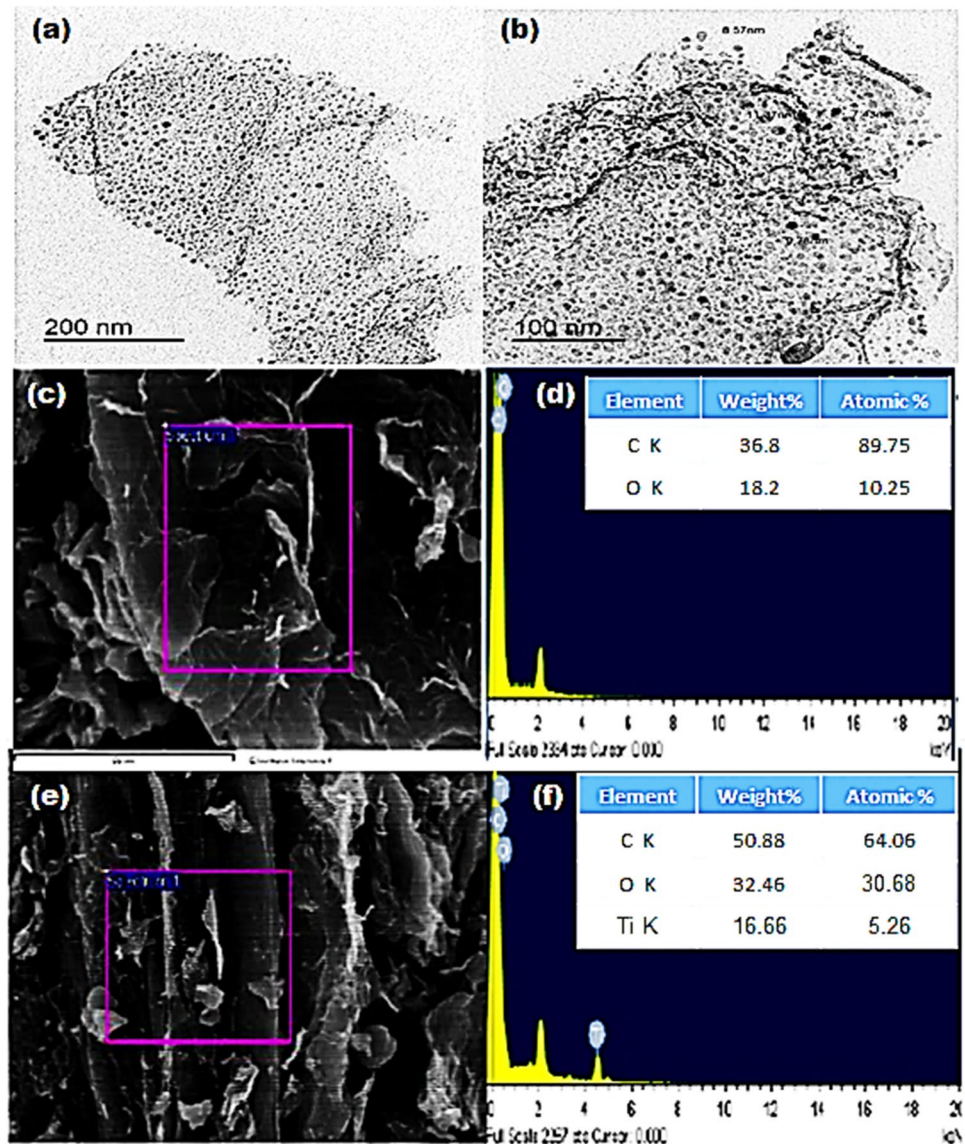
The internal molecular structures of the GO, rGO, TiO<sub>2</sub>, and 50rGO/50TiO<sub>2</sub> samples are studied using FTIR as shown in Fig. 2. The large peak that appears at 3454 cm<sup>-1</sup> belongs to the –OH and –COOH groups, whereas the peaks at 1730, 1442, 1260, and 1067 cm<sup>-1</sup> belong to the C=O, C=C (and –OH), C–O–C, and –OH groups, respectively. These peaks appear from the incorporation of the functional groups containing oxygen (hydroxyl, carbonyl, carboxylic, and epoxide groups) into the basal graphite sheets, increasing interplanar separation. In addition, after hydrothermal treatment in rGO, the peak intensity reduces considerably or even disappears, showing that the rGO nanosheets are successfully modified by hydrothermal treatment. In TiO<sub>2</sub>, a broad peak between 500 and 900 cm<sup>-1</sup> relates to the vibration of Ti–O–Ti bonds (Gu et al. 2013; Mino et al. 2016). The intensity of the peak associated with hydroxyl and epoxy groups (C–O) is reduced in the 50rGO/50TiO<sub>2</sub> sample, confirming the successful anchoring of TiO<sub>2</sub> in the rGO nanostructure (Pastrana-Martinez et al. 2014; Liu et al. 2016; Cruz et al. 2017).

Figure 3a and b shows the TEM images of the 50rGO/50TiO<sub>2</sub> nanocomposite samples with different magnifications. It is evident that there is a uniform distribution



**Fig. 2** The FTIR spectra for the GO, the rGO, TiO<sub>2</sub> nanoparticles, and 50 rGO/50TiO<sub>2</sub> nanostructures

**Fig. 3** **a** and **b** TEM image of 50 rGO/50TiO<sub>2</sub>, **c** and **d** SEM image with EDX of pure rGO nanosheets, **e** and **f** SEM image with EDX for the 50rGO/50TiO<sub>2</sub> nanocomposite sample



of TiO<sub>2</sub> in the rGO nanosheet. The average diameter of TiO<sub>2</sub> nanoparticles within the sheet has been counted using Image J software to be c.a. 10 nm. SEM and EDX analysis have been performed to verify the chemical composition of the samples under consideration. Figure 3c to f shows the EDX characterization of the rGO and 50rGO/50TiO<sub>2</sub> hybrid based on the SEM picture. Regarding the SEM pictures (Fig. 3c and e), the difference is that the surface is smooth for pure rGO, while in Fig. 3e, the presence of TiO<sub>2</sub> nanoparticles attached to the rGO nanosheet makes the surface relatively rough. The EDX analysis showed the presence of C atoms with some O atoms, as shown in Fig. 3d and depicted in the inserted table. In contrast, the presence of Ti atoms in the test for the 50rGO/50TiO<sub>2</sub> sample in Fig. 3f indicates the presence of TiO<sub>2</sub> on the rGO surface.

X-ray photoelectron spectroscopy (XPS) can provide significant evidence about a material's surface chemical

structure. The XPS spectra of the C1s, O1s, and Ti2p regions of 50rGO/50TiO<sub>2</sub> composite materials and pure TiO<sub>2</sub> are shown in Fig. 4. The XPS spectra survey shown in Fig. 4a, while b, c, and d indicate the high resolution presence of C, O, and Ti in the nanocomposite material, which supports the formation of TiO<sub>2</sub> anchored to the rGO nanosheets. The XPS of pure TiO<sub>2</sub> is also fitted with peaks corresponding to titanium dioxide in Ti 2p<sub>1/2</sub> and Ti 2p<sub>3/2</sub>, respectively. These peaks are fitted as Ti 2p<sub>1/2</sub> at 463.9 eV and Ti 2p<sub>3/2</sub> at 458.15 eV. The line separation between Ti 2p<sub>1/2</sub> and Ti 2p<sub>3/2</sub> is 5.75 eV, which is consistent with the standard binding energy of TiO<sub>2</sub> (Bharti et al. 2016). The C1s spectrum is convoluted into four peaks, each with BEs of 284.37, 285.46, and 289.93 eV, corresponding to C–C, C–O, and C=O bonds. Also, the presence of Ti<sup>4+</sup> in the high-resolution Ti2p spectrum indicates that the TiO<sub>2</sub> remains in its distinctive crystal structure during the procedure. Furthermore, in Fig. 4d, the

**Fig. 4** **a** The XPS spectra of both TiO<sub>2</sub> nanoparticles and 50 rGO/50 TiO<sub>2</sub> photocatalyst, **b** C1s, **c** O1s, and **d** Ti2p regions

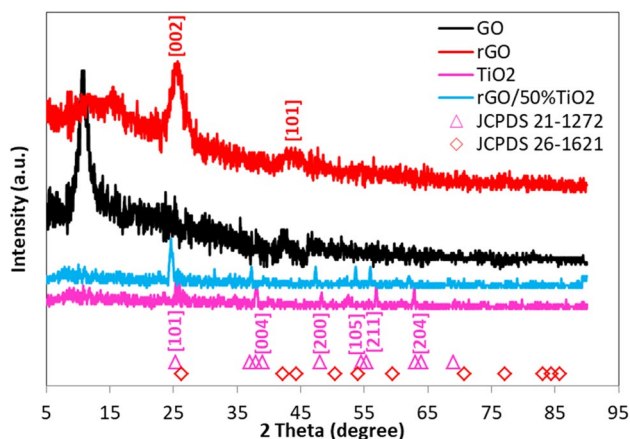
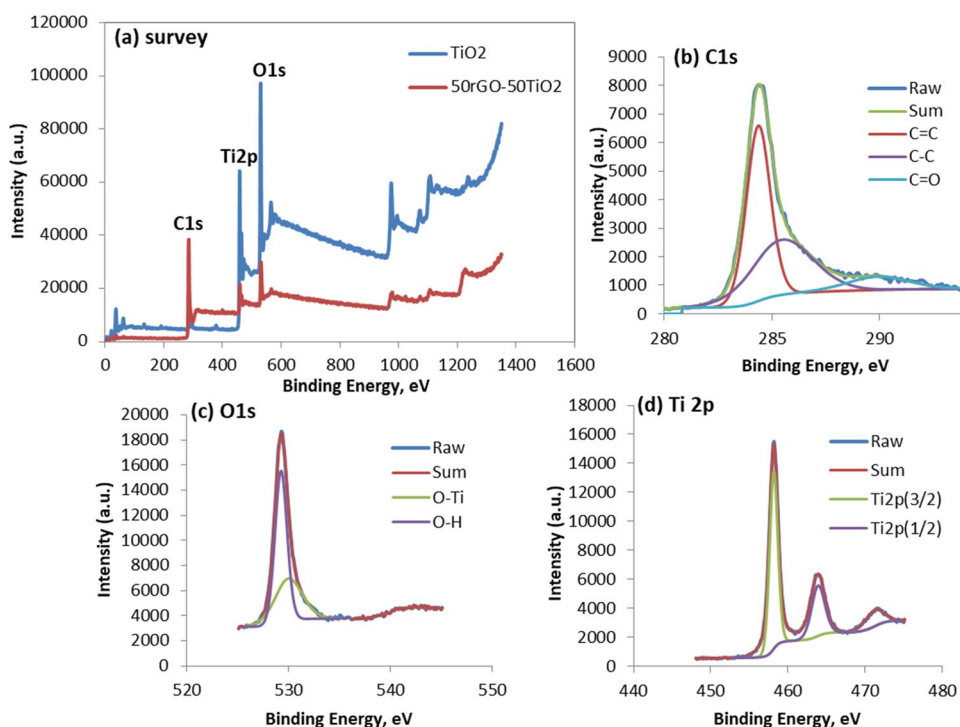


**Fig. 5** XRD of TiO<sub>2</sub>, GO, rGO, and 50 rGO/50TiO<sub>2</sub> nanostructures

O–Ti bond in TiO<sub>2</sub> is assigned bands with energies of 458.15 eV (Ti 2p<sub>3/2</sub>) and 463.34 eV (Ti 2p<sub>1/2</sub>) (Fan et al. 2011; Xu et al. 2011; Appavoo et al. 2014; Lim et al. 2019; Ruidíaz-Martínez et al. 2020).

The phase structure of the resulting samples can be analyzed using XRD. Figure 5 illustrates the X-ray of TiO<sub>2</sub>, GO, rGO, and 50rGO/50TiO<sub>2</sub> samples. Also, the figure shows the peak points obtained from the JCPDS cards for anatase TiO<sub>2</sub> and rGO. The GO diffractogram shows only two peaks at 2θ values of 10.5° and 42.5° similar to previous studies (Ismail et al. 2013). Individual GO sheets are expected to be thicker than the original graphene due to the presence of

oxygen-containing functional groups bound to both sides of the sheets and the roughness at the atomic scale caused by structural defects (sp<sup>3</sup> bond) generated in the originally flat graphene sheets (Shen et al. 2011; Sher Shah et al. 2012). So, this observation proves that after the hydrothermal treatment by plant extract, the GO sample is reduced to rGO acceptably. For the TiO<sub>2</sub> nanoparticles, they exhibited peaks at 25.51° (101), 37.7° (004), 47.6° (200), 53.3° (105), 57.1° (211), and 62.74° (204) which agree with the JCPDS 21-1272 card and are also in line with that obtained by Zhang et al. (2010), Cheng et al. (2012), and Hafeez et al. (2018). For the 50rGO/50%TiO<sub>2</sub> nanocomposite sample, because of the low intensity of the peaks and their overlap with the strong anatase peak at 24.6°, no diffraction peak similar to rGO at 2θ ≈ 25.0° was found in the XRD pattern of the 50rGO/50TiO<sub>2</sub> nanocomposite sample (Yang et al. 2008; Park et al. 2011; Hajjalilou et al. 2021). Due to the high quantity of TiO<sub>2</sub>, the curve of 50rGO/50%TiO<sub>2</sub> nanocomposite sample is close in its shape to the curve of pure anatase TiO<sub>2</sub>.

The UV-vis absorption spectra of rGO, TiO<sub>2</sub>, and 50rGO/50TiO<sub>2</sub> are displayed in Fig. 6a. Pure TiO<sub>2</sub> can only absorb light with a wavelength of less than 400 nm. The peak site of rGO doped with TiO<sub>2</sub> gradually shifted to higher wavelengths. The peak's red shift suggested that it has gained notable absorption characteristics relative to both pure TiO<sub>2</sub> and rGO (Siong et al. 2019). To calculate the bandgap of the prepared sample, Fig. 6a inset shows a plot of the (αhν)<sup>2</sup> versus the photon energy (hν), where α is

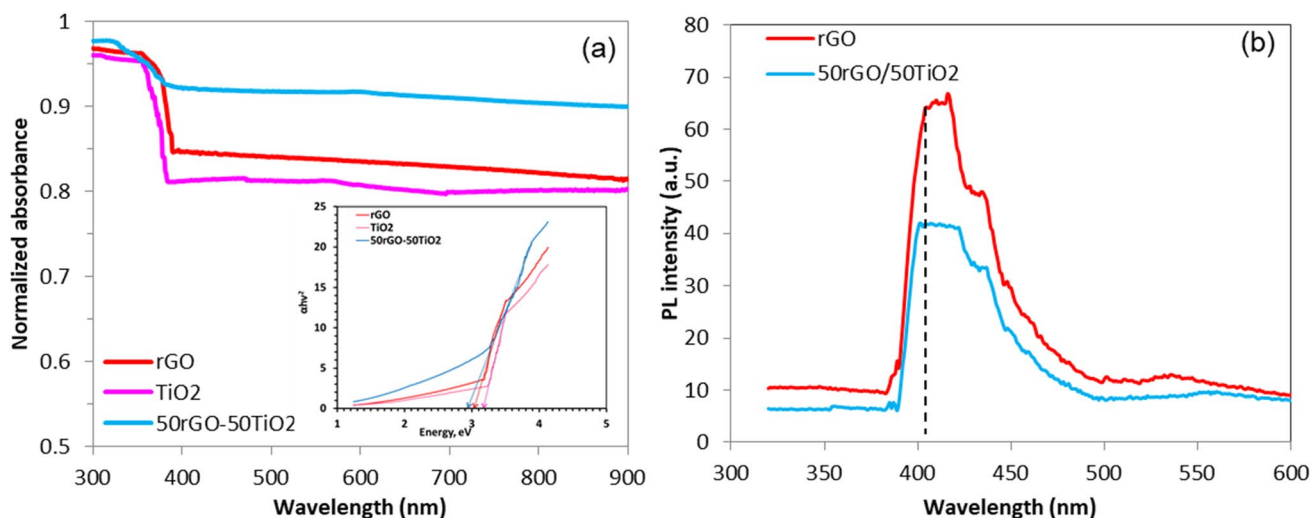


**Fig. 6** **a** DRS, (inset) band gap calculation for the three samples, and **b** PL of rGO and 50 rGO/50TiO<sub>2</sub> photocatalyst

the optical absorption coefficient. It can be calculated from normalized absorbance and the thickness of the sample ( $t$ ) using  $\alpha = 2.303A/t$ . The value of  $h\nu$  can be calculated from wavelength using  $h\nu = 1240/\text{wavelength}$ . Extrapolating the linear portion of the curves to the x axis will give the value of the energy band gap. It is shown in the inset of Fig. 6a that the band gap value for TiO<sub>2</sub>, rGO, and 50%rGO-50%TiO<sub>2</sub> nanocomposite are 3.2, 3, and 2.9 eV, respectively. Comparing the band gap values of this study with the reported values showed that the band gap of the 50%rGO-50%TiO<sub>2</sub> nanocomposite has been slightly decreased. Thus, it should reveal better photocatalytic activity under visible light radiation. This band gap narrowing of TiO<sub>2</sub> has also been reported for other components like TiO<sub>2</sub>/NrGO and TiO<sub>2</sub>/CNT nanocomposite (Zhang et al. 2010; Lin et al. 2017).

Photoluminescence is commonly used to assess the surface structure and excited state of semiconductors, as well as to investigate electron-hole pair recombination. The emission spectra of the PL of the sample materials are depicted in Fig. 6b. It is evident that the luminescence efficiency of the 50rGO/50TiO<sub>2</sub> composites is lower than that of the rGO, indicating the depressed recombination of the electron-hole pairs in the 50rGO/50TiO<sub>2</sub> nanocomposite sample (Alamelu et al. 2018; Tang et al. 2018). At 420 to 500 nm, a few other peaks with varying intensities are observed, which could be attributed to Schottky barrier formation at metal nanoparticle and substrate interfaces (Liu et al. 2018; Cheng et al. 2017). An explanation of that might be due to a higher concentration of graphene that affects the surface active sites of TiO<sub>2</sub> photocatalysts, hiding them from incident photons and resulting in a small decrease in H<sub>2</sub> production. According to the observations, enhancing the photocatalytic performance of graphene–TiO<sub>2</sub> composites for efficient hydrogen

production and pollutant decomposition requires an optimum loading of graphene to TiO<sub>2</sub> (Wang et al. 2017).

### Photocatalytic water splitting and methylene blue decomposition

Figure 7a displays the hydrogen production rate vs. time for GO, rGO, TiO<sub>2</sub>, and nanocomposite with varying percentages of TiO<sub>2</sub> and rGO. It is worth mentioning that the concentration of MB dye was kept at 100 ppm and the flask was stirred at 100 rpm to overcome the diffusion barrier to and from the photocatalyst surface. It is noticeable that two sets of curves appear; the first one for pure GO, rGO, and TiO<sub>2</sub> photocatalysts, while the second set is for the nanocomposite photocatalysts. The rate of hydrogen production increases with time, indicating that the rate of hole consumption, due to the valence band reaction or the organic scavenger, is higher in the presence of MB than without it. The rate of hydrogen production for the 50rGO/50TiO<sub>2</sub> nanocomposite sample reaches 224.9  $\mu\text{mol}/\text{min g}_{\text{catalysts}}$ . It is also interesting to monitor the effect of the addition of the MB dye on the rate of hydrogen production. Figure 7b shows the rate of hydrogen production vs. time in the presence of MB dye and using different masses of the 50rGO/50TiO<sub>2</sub> nanocomposite. It can be seen that the average rate of hydrogen generation in the first stage was common for the three masses at c.a. 572  $\mu\text{mol}/\text{min g}_{\text{catalysts}}$ , proving that the photocatalyst can conjointly stimulate both photo-degradation of the MB dye and H<sub>2</sub>O splitting reactions. This was true for the first 120 min, after which the rate of hydrogen generation dropped dramatically to 8.52  $\mu\text{mol}/\text{min g}_{\text{catalysts}}$  due to the consumption of the majority of the MB scavenger in the reaction, as shown in the inset of Fig. 7b.

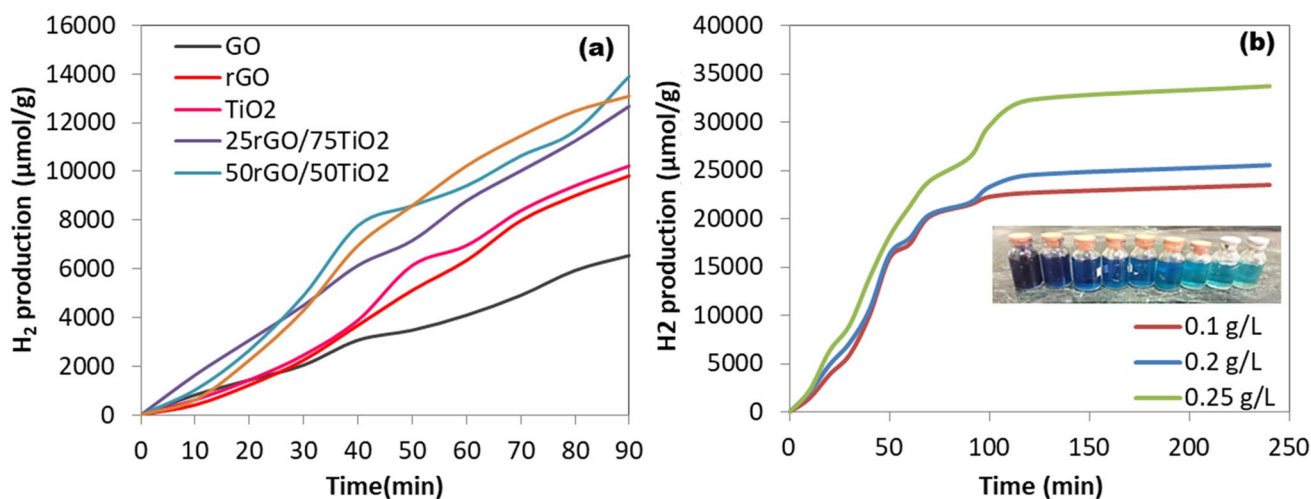


**Fig. 7** **a** Photocatalytic H<sub>2</sub> production rates different concentration of catalyst. Conditions: 0.005 g of catalysts, 100 ppm of MB solution, 200 rpm, 2000-W Hg lamp. **b** Photocatalytic H<sub>2</sub> production rates over

the 50rGO/50TiO<sub>2</sub> catalyst. Inset: A picture shows the decrease in the MB dye concentration with time. Conditions: mass of catalyst (0.1, 0.2, and 0.25 g/L), [MB] = 100 ppm, rpm = 200, 2000-W Hg lamp

The reaction mechanism that happens over the nanocomposite photocatalyst can be subdivided into several steps. Once the catalyst is inserted into the reaction flask, MB molecules will be adsorbed over the surface of the photocatalyst due to electrostatic attraction between the TiO<sub>2</sub> active sites and the MB dye molecules. As for the MB-titania interaction, the electrostatic attraction is expressed as follows (Wang et al. 2012).



where \* represents the adsorption sites over the surface of the photocatalyst. The number of MB molecules adsorbed depends on the number of active sites available for adsorption both on the surface and in the pores of the catalysts. Since all the photocatalyst nanoparticles have the same surface structure, it is expected that MB adsorption will be approximately the same for all the photocatalyst nanoparticles. It is expected that the MB adsorption will not be done over the entire surface of the photocatalyst. Only the hydrolyzed surfaces that contain active –OH groups are the favorite sites for such connections (Wang et al. 2012). Generally, the surface of TiO<sub>2</sub> nanoparticles is hydrophilic while the rGO surfaces are hydrophobic. However, due to the chemical reduction routes that have been used, an incomplete reduction of GO to rGO happens, and some remote areas appear to have some remaining active oxygen sites that can equally act as hydrophilic sites. The hydrated MB molecules prefer attachment to the hydrophilic sites of the nanocomposite (both TiO<sub>2</sub> nanoparticles and the remote rGO sites). Accordingly, MB acts as a local hole scavenger on the valence band of TiO<sub>2</sub> and some remote sites of the

rGO nanosheet. Thus, an equal loading of TiO<sub>2</sub> and rGO is anticipated to produce the maximum hydrogen production rate, which is in agreement with the experimental findings.

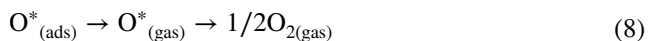
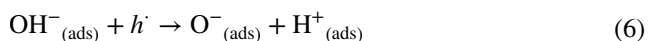
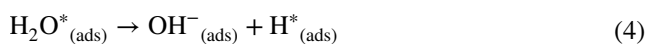
As indicated in Fig. 6a, the visible light absorption has been enhanced by doping rGO with TiO<sub>2</sub> nanoparticles. It is also expected that the porosity of the prepared nanocomposite will be enhanced. Therefore, the absorption of more photons over the surface of the 50rGO/50TiO<sub>2</sub> nanocomposite sample improves its ability to decompose the MB molecules. Accordingly, the synergetic effects of high porosity and optical band gap are the key factors for enhancing the photocatalytic activity of the 50rGO/50TiO<sub>2</sub> nanocomposite photocatalyst.

Upon irradiation of the nanocomposite in the solution containing the MB dye, photoexcitation of the electrons from the conduction to valence band happens over the surface of TiO<sub>2</sub> nanoparticles (Eq. 2).



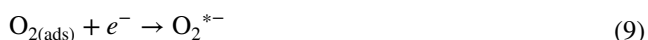
The recombination between the photon-generated *eh* pairs can happen normally within microseconds (Wilke and Breuer 1999). However, two parallel mechanisms are hindering such fast recombination. The first mechanism involves the presence of the p-n junction between TiO<sub>2</sub> nanoparticles and the rGO nanosheet, which will cause the movement of the holes to the adjacent surface of rGO while the electrons will be accumulated on the conduction band of the TiO<sub>2</sub> nanoparticles. This scenario will provide a path for the fast hydrogen evolution reaction and the sluggish oxygen reduction reaction to simultaneously happen according to the following sub-reactions (Nowotny et al. 2005).





When the surface of the nanocomposite is illuminated by solar beams, the photocatalyst is capable of acquiring the excitation energy from the light source due to the narrowed band gap, leading to the instantaneous appearance of excited  $e/h$  pairs. As indicated in Eq. (4), the adsorbed water molecule reacts to form a highly reactive  $\text{OH}^-_{(\text{ads})}$  over the catalyst surface. In the conduction band, the adsorbed hydrogen radical can accept the electron and form an adsorbed hydrogen atom, which in turn combines with another atom to form a hydrogen molecule. The  $\text{OH}^-_{(\text{ads})}$  radical splits at the valence band site in the presence of a hole to form  $\text{O}^-_{(\text{ads})}$  and  $\text{H}^+_{(\text{ads})}$ , as shown in Eq. (6). A subsequent reaction between a hole and the  $\text{O}^-_{(\text{ads})}$  atom forms an adsorbed oxygen radical. This in turn reacts with another radical to form an adsorbed oxygen atom (Eqs. 7 and 8).

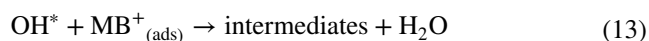
However, another set of reactions are simultaneously proceeding in parallel with reactions (Eqs. 6–8), that is, the decomposition of MB dye over the valence band of  $\text{TiO}_2$  (and the remote rGO sites). The reduction of MB molecules under visible light irradiation is considered a surface-catalyzed reaction, which depends on the number of adsorbed MB molecules. The rate of adsorption and desorption of the MB molecules will also affect the rate of MB decomposition, as will be indicated in the next part. In the parallel reactions, oxygen molecules accept electrons and form super oxide anion radicals:



The oxygen radical anions may act as oxidizing sites or as a stimulator to form of additional hydroxyl radicals by a sequence of reactions (Wang et al. 2012):



The hydroxyl radicals formed react with the adsorbed MB molecules and catalyze the photodecomposition of the molecules to colorless intermediates (Eq. (13)). The sequence of MB decomposition consists of several steps which are not indicated here.



### Kinetic study for the photocatalytic MB decomposition

Organic dyes are typically used in industrial coloring and printing applications. They are frequently found in industrial wastewater, presenting an environmental risk. Dye decomposition produced harmful chemicals, resulting in water contamination that harmed humans and creatures. Because photon-induced water splitting and organic decomposition are heterogeneous reactions, they involve multiscale physicochemical and photo-electrochemical processes such as fluid flow interactions, optical response, surface reaction kinetics, and heat and mass transfer (Dong et al. 2021). It is essential to understand the rate-controlling step for such reactions for better scale-up and design. A macrokinetic study for the photocatalytic activity of the photocatalyst toward MB decomposition has been performed. The study was carried out using different percentages of the nanocomposite photocatalyst (rGO– $\text{TiO}_2$ ). The photocatalytic decomposition of MB dye has been tested using a UV-vis spectrophotometer. The experiment was carried out in the presence of a mercury light source. Under a mercury lamp, photocatalysis of adsorbed MB molecules happens on the surface of the catalyst, which affects the number of adsorptive sites and optical band gap of nanocomposite catalysts.

Furthermore, the ratio between final concentration ( $C_t$ ) and initial concentration ( $C_o$ ) was used to calculate the decomposition efficiency. The following formula was used to compute the MB decomposition percentage (Ramar et al. 2018; Ramar and Balasubramanian 2021):

$$\frac{C_o - C_t}{C_o} \times 100\% \quad (14)$$

The rate of MB concentration change can be determined from:

$$dC_t/dt = -kC_t^n \quad (15)$$

where  $C_t$  is the concentration of MB in kmol/L,  $k$  is a pseudo rate constant, and  $n$  is the reaction order. The linear form of Eq. (15) is:

$$\ln(-dC_t/dt) = \ln k + n \ln C_t \quad (16)$$

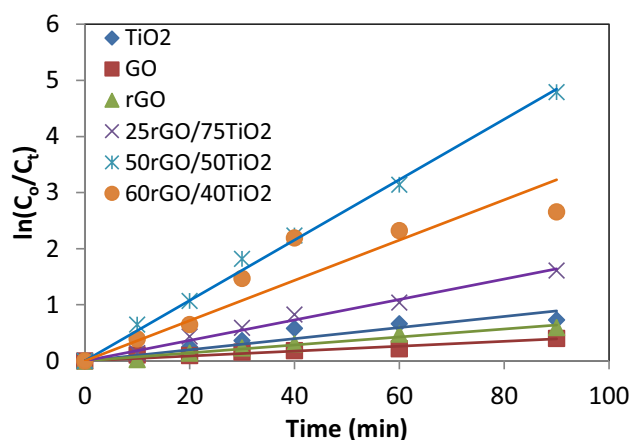


**Fig. 8**  $\ln(C_0/C_t)$  vs. time for different nanocomposite catalyst for the decomposition of MB dye

**Table 1** Effect of different nanocomposite catalyst on photocatalytic decomposition efficiency and photocatalytic decomposition rate of MB dye

Catalyst	Photocatalytic decomposition efficiency (%)	$k$ ( $\text{min}^{-1}$ )	$R^2$
TiO <sub>2</sub>	51.70423	0.0099	0.8467
GO	32.8806	0.0043	0.9314
rGO	44.7083	0.0071	0.9736
25rGO/75TiO <sub>2</sub>	79.98008	0.0182	0.9881
50rGO/50TiO <sub>2</sub>	99.17158	0.0538	0.9955
60rGO/40TiO <sub>2</sub>	92.97593	0.0359	0.8344

For the MB decomposition reaction, the pseudo-first-order kinetic plots were used to investigate the decomposition rate constant ( $k$ ) of the produced catalyst. Starting from Eq. (16), the rate constant values of the samples were estimated using the following expression (Sultana et al. 2018; Ramar and Balasubramanian 2019).

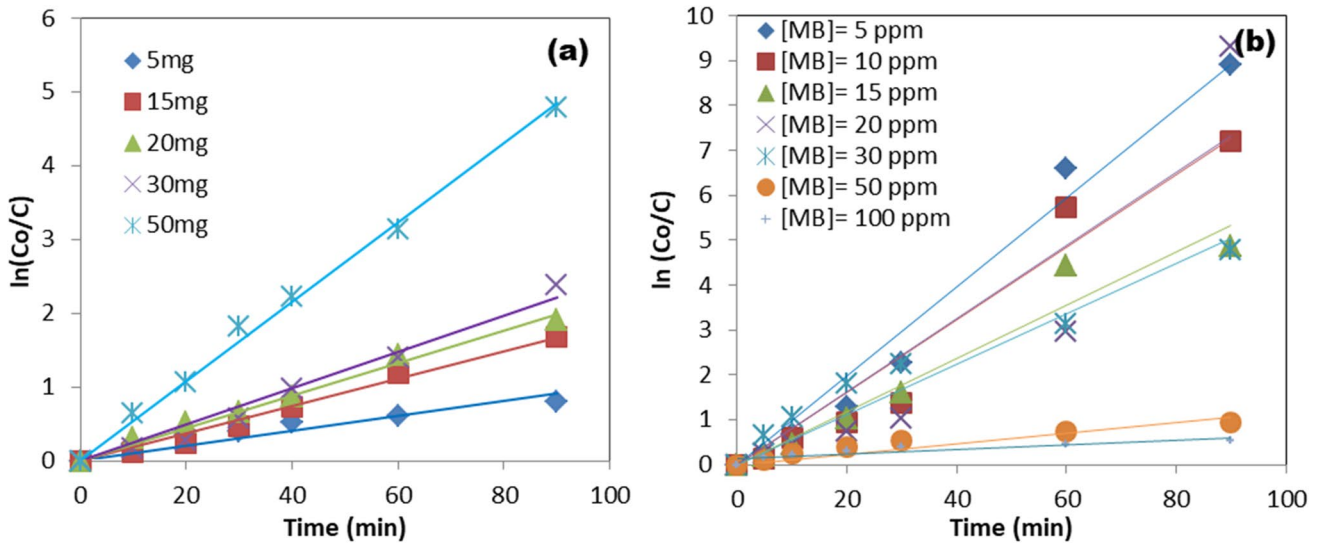
$$\ln(C_0/C_t) = k \times t \quad (17)$$

Figure 8 plots  $\ln(C_0/C_t)$  versus  $t$  for different photocatalysts. It is noticeable that the presence of composite materials significantly improves the MB dye removal, and the decomposition rate constant is raised from  $0.0099 \text{ min}^{-1}$  using TiO<sub>2</sub> nanoparticles to  $0.0538 \text{ min}^{-1}$  using 50rGO/50TiO<sub>2</sub> nanocomposite. The large increase in rate constant values compared to the pure photocatalysts indicates that the photocatalytic activity has been improved by using the p-rGO/n-TiO<sub>2</sub> nanocomposite. As shown in Table 1, the presence of TiO<sub>2</sub> doped into the rGO nanosheets has augmented the photocatalytic activity of TiO<sub>2</sub> and rGO as well as improved the adsorption capacity. It is also noticeable that the photocatalytic

activity of composite materials is influenced by the rGO content. Thus, as the mass ratio of rGO to TiO<sub>2</sub> rises from 0 to 50%, the dye removal percentage also increases. But the removal percentage decreases again using the sample of 60%rGO/40%TiO<sub>2</sub> photocatalyst. This drop affects the photodecomposition process performance because both materials have a synergic effect on pollutant adsorption and photocatalysis. When this optimal rGO amount is exceeded, the performance of the process decreases because an excess of rGO particles can surpass the active sites on the TiO<sub>2</sub> surface and act as recombination centers (Jiang et al. 2011; Long et al. 2013; Awfa et al. 2018; Petala et al. 2019). The calculated decomposition percentages using different amounts of the photocatalysts after 90 min of the reaction are shown in Table 1. The 50rGO/50TiO<sub>2</sub> sample induced the maximum MB decomposition percentage. This could be attributed to two probable reasons. Firstly, the light source that has been used in this study is not capable of generating a sufficient quantity of  $e/h$  pairs. Consequently, it will incompletely stimulate the photocatalytic reaction on part of the adsorbed MB over TiO<sub>2</sub> active sites. Secondly, it is clear from Eqs. 2–13) that the photocatalysis is a complicated series/parallel reaction exhibiting a higher energy barrier than the MB physical adsorption step over the adsorptive sites. At the TiO<sub>2</sub> sites, the energy required for inducing  $e/h$  pair excitation is in the range of 2.4–3.2 eV, which is higher than the physisorption energy requirement of c.a. 0.1 eV (Jaramillo-Fierro et al. 2021). This means that the rate-determining step for MB decomposition is appearing in the photocatalytic reactions (photon adsorption, electron/hole generation, radical formation, and MB decomposition).

Figure 9a shows the influence of the mass of the photocatalyst (5 to 50 mg) on the rate of dye removal. It is evident that the MB deterioration fits a pseudo-first-order equation for photocatalytic dye decomposition. Moreover, Table 2 shows the percentages of MB decomposition,  $k$ , and  $R^2$  values in the presence of different masses of the photocatalyst. It is evident that employing 50 mg of the photocatalyst resulted in the highest mass transfer due to the presence of a vast number of active sites for the photocatalytic reaction; therefore, utilizing such a large amount of catalyst practically resulted in the full removal of the MB dye within 90 min. Hence, 50 mg was considered as the optimum catalyst loading for this work.

Figure 9b displays the effect of different initial MB concentrations on the efficiency of the 50rGO/50TiO<sub>2</sub> photocatalyst. It was evaluated using different initial MB solution concentrations ranging from 5 to 200 ppm. At most of the MB concentrations, the rate of dye removal follows a linear form, indicating that the reaction over



**Fig. 9** a Effect of mass of the 50rGO/50TiO<sub>2</sub> photocatalyst on the photocatalytic decomposition of MB dye ([MB]= 50 ppm). b Effect of initial MB dye concentration on the photocatalytic activity of 50 mg of the 50rGO/50TiO<sub>2</sub> photocatalyst

**Table 2** Effect of catalyst loading and initial dye concentration on photocatalytic decomposition efficiency and photocatalytic decomposition rate of MB dye

Photocatalyst mass (mg/L)	MB dye concentration (ppm)	Photocatalytic decomposition efficiency (%)	<i>k</i> (min <sup>-1</sup> )	Reaction time, min
5	30	55.36	0.0103	90
15	30	81.46	0.0185	90
20	30	83.57	0.0221	90
30	30	88.44	0.0246	90
50	5	99.98	0.1109	60
50	10	99.92	0.0896	60
50	15	99.23	0.0682	60
50	20	99.99	0.0742	60
50	30	99.17	0.0538	60
50	50	61.35	0.0114	90
50	100	41.78	0.0072	90
50	200	27.42	0.0042	90

the photocatalyst sites was mainly the rate-controlling step. The MB molecules adsorbed on the adsorbent/photocatalyst surface prevented more MB molecules from reaching the adsorbent/photocatalyst surface, resulting in a decrease in MB removal. Furthermore, a high initial MB concentration hampered visible light penetration due to increased turbidity, which reduced the light irradiation effect for photocatalytic destruction of MB (Ba-Abbad et al. 2013; Tran Thi et al. 2019). More dye molecules accumulate on the catalyst surface as the initial concentration of dye solution increases. The existing adsorption sites eventually become saturated and unable to handle the growing number of dye molecules. Due

to the shorter path length of photons into the solution, the photocatalytic decomposition rate was reduced as the initial concentration of dye increased, according to the Beer–Lambert equation (Anku et al. 2016; Siong et al. 2019).

Based on the data in Table 2, the value of the reaction rate constant can be expressed as a function of catalyst mass and initial dye concentration according to the following equation:

$$k = 0.17 \times m^{0.74} \times C^{-0.58} \tag{18}$$

where *m* is the mass of the photocatalyst in mg and *C* is the initial dye concentration. Equation (18) indicates the high

**Table 3** Survey of some reported photocatalysts used for photocatalytic decomposition of some dyes

Nanomaterial used	Dye type	Decomposition %	Reaction time	Light source	Ref
RGO/Cu	50 mL of 5 ppm mix rhodamine B (RhB)	91.0%	60 min	UV lamp	Safajou et al. (2021)
BiOBr-G	50 mL of $2 \times 10^{-5}$ M MB	96.41%	75 min	5-W white light light-emitting diode lamp visible light	Shih et al. 2021
GO–ZnO–Ag	100 mL of MB ( $3.13 \times 10^{-5}$ M), pH 6.5	100%	90 min	Sunlight	Al-Rawashdeh et al. (2020)
rGO/Ag	(5 mg/500 mL) MB	100%	120 min	Mercury lamp 400 W	Ikram et al. (2020)
7%rGO-TiO <sub>2</sub>	(0.3 mM) with 0.7 g/L ethylparaben (EtP)	98.6%	40 min	Medium-pressure mercury vapor lamp (150 W)	Ruidíaz-Martínez et al. (2020)
rGO(1.0 wt%)-TiO <sub>2</sub>	MB	97%	60 min	Hg lamp of 450 W	Singh et al. (2020b)
Ag-ZnO/GO	20 mL of MB 15 mg/L	99%	180 min	UV lamp	Tran Thi et al. (2019)
ZnO/rGO	50 mL MB solution (40 mg/L).	~100%	80 min	350-W xenon lamp	Liu et al. (2020)
rGO-160	50 ppm of dye at pH 11, 100 mL	98.57%	6 h	UV-C light ( $2 \times 95$ W; intensity $60 \text{ W m}^{-2}$ )	Siong et al. (2019)
ZnO spindle/reduced graphene	10 mg/L MB	93%	180 min	500-W halogen lamp visible light	Prabhu et al. (2018)
NiFe <sub>2</sub> O <sub>4</sub> -reduced graphene oxide	(20 mg/L) 40 mL MB	99.1%	180 min	800-W Xe lamp UV irradiation	Liang et al. (2018)
rGO/ZnO (nanorod)	RhB, MO, MB, and aqueous solution (10 mg/L)	MB 93.9%, RhB 88.08%, MO 75.3%	180 min	75-W xenon lamp visible light	Ranjith et al. (2017)
BiVO <sub>4</sub> /Ag/rGO	10 ppm MB	90%	140 min	300-W xenon lamp	Patil et al. (2017)
CoFe <sub>2</sub> O <sub>4</sub> -rGO	(20 mg/L) 40 mL MB	96.8%	3 h	800-W Xe lamp	He et al. (2015)
NiFe <sub>2</sub> O <sub>4</sub> -graphene	(20 mg/L) 100 mL MB	~100%	3 h	500-W Xe lamp	Fu et al. (2012a)
MnFe <sub>2</sub> O <sub>4</sub> -graphene	(20 mg/L) 100 mL MB	~99%	6 h	500-W Xe lamp	Fu et al. (2012b)
CoFe <sub>2</sub> O <sub>4</sub> -graphene	(20 mg/L) 100 mL MB	~100%	4 h	500-W Xe lamp	Fu et al. (2012c)
rGO/TiO <sub>2</sub>	$2.5 \times 10^{-5}$ M, pH = 5.8 MB		60 min	Visible light four 20-W lamps	Nguyen-Phan et al. (2011)
rGO-wrapped TiO <sub>2</sub>	(10 mg/L) 50 mL	100%	150 min	Hg lamp, Philips HOK lamps, 400-W UV irradiation	Liu et al. (2011)
50rGO/50TiO <sub>2</sub> prepared by hydrothermal method	(30 mg/L) 100 mL solution MB	100%	90 min	Hg lamp (2000 W)	This work

dependency of the reaction rate on the mass of catalyst rather than the initial dye concentration. This finding implies that photocatalytic reactions are mainly controlled by charge separation, transfer, and surface reaction rather than the diffusion of reactants and products to and from the surface of the photocatalyst. However, the effects of other variables should also be considered, like temperature and boundary layer effects. It can also be suggested that 50rGO/50TiO<sub>2</sub> is the optimum combination that can be used for the purification of water from organic dyes.

Table 3 depicts a general comparison of the photocatalytic decomposition of dyes in the last 10 years. In this table, we have only reported the studies involving using

rGO-based photocatalysts for dye decomposition. The data obtained in this work is comparable to that obtained by Liu et al. (2011). They indicated that adsorption of MB dye first happens with an adsorption capacity of 19.6 mg/g. This process is an irreversible process where the adsorbed MB undergoes the decomposition process. They also indicated the same finding that the charge separation and transfer schemes happen due to the surface junction based on the Schottky junction model. Another note is that the combination of TiO<sub>2</sub> and rGO has been reported by several researchers as an effective photocatalyst. This combination gave the best decomposition percentage under different experimental conditions. And so, TiO<sub>2</sub>/

**Table 4** Comparison of different methods for organic matter decomposition

Material	Method	Condition	% removal @ time of reaction	Ref
GOT-H Ti-doped GO Hummers	Photocatalytic decomposition of diphenhydramine	Photocatalyst = 1.0 g/L were placed in a glass reactor	$k_{app} = 52.5 \times 10^{-3} \text{ min}^{-1}$ , after 60 min	Pedrosa et al. 2018 $k_{app} =$ pseudo-first-order reaction kinetic constants
GOT-B Ti-doped GO-Brodie			$k_{app} = 51.3 \times 10^{-3} \text{ min}^{-1}$ , after 60 min	
rGOT-H Ti-doped rGO Hummers	Ozonation	Photocatalyst = 0.14 g/L Pollutant concentration = 90 mg/L of oxalic acid aqueous solution (V = 200 mL, pH = 3)	$k_{app} = 9.87 \times 10^{-3} \text{ min}^{-1}$ oxalic acid conversion after 180 min	
(Fe <sub>3</sub> O <sub>4</sub> @rGO@TiO <sub>2</sub> )	Photo-Fenton	Light source = a 300-W UV-vis lamp equipped with a $\lambda > 400 \text{ nm}$ Pollutant concentration = 10 mg/L MB	99.0% after 2 h	Yang et al. 2015a
TiO <sub>2</sub> -G film electrode	Photo-electro-Fenton (PEF)	Different scavengers 1,4-benzoquinone, ethylene diamine tetraacetic acid, and tert-butyl alcohol	85.86% within 45 min	Kaur et al. 2020
TiO <sub>2</sub> /graphite felt	UV-driven electro-Fenton	Catalytic membrane florfenicol concentration = 14 $\mu\text{Mol}$	98 $\pm$ 1.9% 120 min	Jiang et al. (2020)
Iron sludge-graphene catalyst	Fenton process	Pollutant name: rhodamine B, acid red G, and metronidazole	RhB removal by: Fe-G-0.5 = 99.0% Fe-G-1 = 98.5% at 120 min	Guo et al. (2017)
FeO-Fe <sub>3</sub> O <sub>4</sub> -rGO	Fenton catalysts	Photocatalyst = 0.10 g/L Pollutant concentration = 50 mg/L MB	98% removal in 60 min	Yang et al. 2015b
Fe <sub>3</sub> O <sub>4</sub> /rGO NCs	Fenton-like catalysts	Photocatalyst = 0.30 g/L Pollutant concentration = 10 mg/L MB	98.6% in 120 min	Liu et al. (2013)
TiO <sub>2</sub> /graphene oxide	Photocatalytic decomposition	Light source: a xenon lamp 500 W was located inside the reactor Photocatalyst = 0.2 g/L, Volume = 0.5 L. pH = 10 Pollutant concentration = 5 mg/L	99% removal 3 h of reaction time	Kurniawan et al. (2020)
P-doped TiO <sub>2</sub> nanoparticles P/Ti ratio = 0.03	Photocatalytic decomposition	Light source: ultraviolet (UV) lamp 365 nm Temperature (400, 600, and 800 K) Photocatalyst = 0.05 g M = 10 $\mu\text{M}$ , V = 250 mL	$\geq 98 \text{ mol.}\%$ removal after 30 min	Yu (2007)
TiO <sub>2</sub> /rGO	Photocatalytic decomposition	Photocatalyst = 50 mg/L Pollutant concentration = 30 mg/L MB, V = 200 mL	99% removal in 60 min	This work

rGO nanocomposite is a promising photocatalyst to be considered in the scaling up of dye wastewater treatment.

Table 4 indicates the different processes implemented for dye removal by decomposition into other organic

compounds. Compared to other processes, the photocatalytic decomposition process requires less time than current processes like Fenton, photo-Fenton, and Fenton-like processes. The main advantage of the photocatalytic

decomposition is that, in the Fenton processes, the continuous addition of iron ions is necessary to create OH radicals, while in the photo-decomposition process, the OH radical is formed continuously over the surface of the photocatalyst. However, the dye concentration in the case of photo-decomposition is limited to a low concentration range. Therefore, the effect of photocatalyst mass on the dye concentration and the photocatalyst stability should be examined intensively before scale-up of this process.

## Conclusion

To conclude, different ratios of reduced graphene oxide and TiO<sub>2</sub> nanoparticles have been used to produce a p-rGO/n-TiO<sub>2</sub> photocatalyst by a hydrothermal treatment method. These photocatalysts have been characterized by different techniques, and their photocatalytic activity was evaluated for inducing both water splitting and dye decomposition reactions. The rate of photon-induced hydrogen production under the Hg lamp has been measured in the presence of 100 ppm of MB dye to be 25,561.43 mol/g<sub>catalysts</sub>. Moreover, experiments were carried out to determine the efficiency of the prepared photocatalyst toward the decomposition of MB under Hg lamp irradiation. The rate of MB decomposition reaches a maximum when the TiO<sub>2</sub> content is 50% (i.e., 50% rGO/50% TiO<sub>2</sub>), even higher than that observed by using pure rGO and TiO<sub>2</sub> nanoparticles. This photocatalyst attained 99% MB decomposition after 60 min of treatment. According to the experiment conditions, the reaction rate constant can be expressed as a function of catalyst mass and initial dye concentration, where the rate increases as the mass of the catalyst increases, while the reaction rate constant is inversely affected by the concentration of MB. The dual action of the photocatalyst is affected by the spectrum of the light source and the rate of the sub-reactions contributing to the decomposition of the organic pollutants. The kinetic study showed that the rate-determining step for MB decomposition is appearing in the photocatalytic reactions (photon adsorption, electron/hole generation, radical formation, and MB decomposition). The results indicate the potential of TiO<sub>2</sub>-doped rGO as an effective photocatalytic for the production of hydrogen and photocatalytic decomposition of MB, which could continue as a potential application for simultaneous wastewater treatment and energy production.

**Author contribution** Hager M. Moustafa: experimentation and analysis, writing—original draft preparation (60%). Mohamed S. Mahmoud: interpreting kinetic study part, writing—reviewing and editing (20%). Mamdouh M. Nassar: conceptualization, interpreting characterization part (20%).

**Data availability** Experimental data are available upon request.

## Declarations

**Ethics approval** This manuscript has no ethical approvals (not applicable).

**Consent to participate** Not applicable to this manuscript.

**Consent for publication** Not applicable to this manuscript.

**Competing interests** The authors declare no competing interests.

## References

- Acharya L, Nayak S, Pattnaik SP, Acharya R, Parida K (2020) Resurrection of boron nitride in pn type-II boron nitride/B-doped-g-C<sub>3</sub>N<sub>4</sub> nanocomposite during solid-state Z-scheme charge transfer path for the degradation of tetracycline hydrochloride. *J Colloid Interface Sci* 566:211–223
- Ahmad M, Ahmed E, Hong Z, Xu J, Khalid N, Elhissi A, Ahmed W (2013) A facile one-step approach to synthesizing ZnO/graphene composites for enhanced degradation of methylene blue under visible light. *Appl Surf Sci* 274:273–281
- Alamelu K, Raja V, Shiamala L, Ali BJ (2018) Biphasic TiO<sub>2</sub> nanoparticles decorated graphene nanosheets for visible light driven photocatalytic degradation of organic dyes. *Appl Surf Sci* 430:145–154
- Al-Mamun M, Kader S, Islam M, Khan M (2019) Photocatalytic activity improvement and application of UV-TiO<sub>2</sub> photocatalysis in textile wastewater treatment: a review. *J Environ Chem Eng* 7(5):103248
- Al-Rawashdeh NA, Allabadi O, Aljarrah MT (2020) Photocatalytic activity of graphene oxide/zinc oxide nanocomposites with embedded metal nanoparticles for the degradation of organic dyes. *ACS Omega* 5(43):28046–28055
- Anku W, Oppong SO-B, Shukla SK, Govender PP (2016) Comparative photocatalytic degradation of monoazo and diazo dyes under simulated visible light using Fe<sup>3+</sup>/C/S doped-TiO<sub>2</sub> nanoparticles. *Acta Chim Slov* 63(2):380–391
- Appavoo IA, Hu J, Huang Y, Li SFY, Ong SL (2014) Response surface modeling of carbamazepine (CBZ) removal by graphene-P25 nanocomposites/UVA process using central composite design. *Water Res* 57:270–279
- Asgharzadeh H, Eslami S (2019) Effect of reduced graphene oxide nanoplatelets content on the mechanical and electrical properties of copper matrix composite. *J Alloys Compd* 806:553–565
- Awfa D, Ateia M, Fujii M, Johnson MS, Yoshimura C (2018) Photodegradation of pharmaceuticals and personal care products in water treatment using carbonaceous-TiO<sub>2</sub> composites: a critical review of recent literature. *Water Res* 142:26–45
- Ba-Abbad MM, Kadhum AAH, Mohamad AB, Takriff MS, Sopian K (2013) The effect of process parameters on the size of ZnO nanoparticles synthesized via the sol-gel technique. *J Alloys Compd* 550:63–70
- Badawy MI, Ghaly MY, Ali ME (2011) Photocatalytic hydrogen production over nanostructured mesoporous titania from olive mill wastewater. *Desalination* 267(2-3):250–255
- Bamwenda GR, Arakawa H (2001) The photoinduced evolution of O<sub>2</sub> and H<sub>2</sub> from a WO<sub>3</sub> aqueous suspension in the presence of Ce<sup>4+</sup>/Ce<sup>3+</sup>. *Sol Energy Mater Sol Cells* 70(1):1–14
- Benjwal P, Kumar M, Chamoli P, Kar KK (2015) Enhanced photocatalytic degradation of methylene blue and adsorption of arsenic (iii) by reduced graphene oxide (rGO)-metal oxide (TiO<sub>2</sub>/Fe<sub>3</sub>O<sub>4</sub>) based nanocomposites. *RSC Adv* 5(89):73249–73260

- Bharatvaj J, Preethi V, Kanmani S (2018) Hydrogen production from sulphide wastewater using  $Ce^{3+}$ -TiO<sub>2</sub> photocatalysis. *Int J Hydrog Energy* 43(8):3935–3945
- Bharti B, Kumar S, Lee H-N, Kumar R (2016) Formation of oxygen vacancies and Ti<sup>3+</sup> state in TiO<sub>2</sub> thin film and enhanced optical properties by air plasma treatment. *Sci Rep* 6(1):1–12
- Boumeriam H, Da Silva ES, Cherevan AS, Chafik T, Faria JL, Eder D (2021) Layered double hydroxide (LDH)-based materials: a mini-review on strategies to improve the performance for photocatalytic water splitting. *J Energy Chem* 64:406–431
- Buliyaminu IA, Aziz MA, Shah SS, Mohamedkhair A, Yamani ZH (2020) Preparation of nano-Co<sub>3</sub>O<sub>4</sub>-coated Albizia procera-derived carbon by direct thermal decomposition method for electrochemical water oxidation. *Arab J Chem* 13(3):4785–4796
- Chen X, Shen S, Guo L, Mao SS (2010) Semiconductor-based photocatalytic hydrogen generation. *Chem Rev* 110(11):6503–6570
- Cheng P, Yang Z, Wang H, Cheng W, Chen M, Shangguan W, Ding G (2012) TiO<sub>2</sub>-graphene nanocomposites for photocatalytic hydrogen production from splitting water. *Int J Hydrog Energy* 37(3):2224–2230
- Cheng K, Han N, Su Y, Zhang J, Zhao J (2017) Schottky barrier at graphene/metal oxide interfaces: insight from first-principles calculations. *Sci Rep* 7(1):1–8
- Cruz M, Gomez C, Duran-Valle CJ, Pastrana-Martinez LM, Faria JL, Silva AM, Faraldos M, Bahamonde A (2017) Bare TiO<sub>2</sub> and graphene oxide TiO<sub>2</sub> photocatalysts on the degradation of selected pesticides and influence of the water matrix. *Appl Surf Sci* 416:1013–1021
- Deb Nath NC, Shah SS, Qasem MAA, Zahir MH, Aziz MA (2019) Defective carbon nanosheets derived from Syzygium cumini leaves for electrochemical energy-storage. *ChemistrySelect* 4(31):9079–9083
- Dong L, Mazzarino I, Alexiadis A (2021) Development of solid–fluid reaction models—a literature review. *ChemEngineering* 5(3):36
- Eidsvåg H, Bentouba S, Vajeeston P, Yohi S, Velauthapillai D (2021) TiO<sub>2</sub> as a photocatalyst for water splitting—an experimental and theoretical review. *Molecules* 26(6):1687
- Fan W, Lai Q, Zhang Q, Wang Y (2011) Nanocomposites of TiO<sub>2</sub> and reduced graphene oxide as efficient photocatalysts for hydrogen evolution. *J Phys Chem C* 115(21):10694–10701
- Fu Y, Chen H, Sun X, Wang X (2012a) Combination of cobalt ferrite and graphene: high-performance and recyclable visible-light photocatalysis. *Appl Catal B Environ* 111:280–287
- Fu Y, Chen H, Sun X, Wang X (2012b) Graphene-supported nickel ferrite: a magnetically separable photocatalyst with high activity under visible light. *AIChE J* 58(11):3298–3305
- Fu Y, Xiong P, Chen H, Sun X, Wang X (2012c) High photocatalytic activity of magnetically separable manganese ferrite–graphene heteroarchitectures. *Ind Eng Chem Res* 51(2):725–731
- Gao Y, Pu X, Zhang D, Ding G, Shao X, Ma J (2012) Combustion synthesis of graphene oxide–TiO<sub>2</sub> hybrid materials for photodegradation of methyl orange. *Carbon* 50(11):4093–4101
- Gopinath KP, Madhav NV, Krishnan A, Malolan R, Rangarajan G (2020) Present applications of titanium dioxide for the photocatalytic removal of pollutants from water: a review. *J Environ Manag* 270:110906
- Gu L, Wang J, Cheng H, Zhao Y, Liu L, Han X (2013) One-step preparation of graphene-supported anatase TiO<sub>2</sub> with exposed {001} facets and mechanism of enhanced photocatalytic properties. *ACS Appl Mater Interfaces* 5(8):3085–3093
- Guo S, Yuan N, Zhang G, Jimmy CY (2017) Graphene modified iron sludge derived from homogeneous Fenton process as an efficient heterogeneous Fenton catalyst for degradation of organic pollutants. *Microporous Mesoporous Mater* 238:62–68
- Guo Q, Zhou C, Ma Z, Yang X (2019) Fundamentals of TiO<sub>2</sub> photocatalysis: concepts, mechanisms, and challenges. *Adv Mater* 31(50):1901997
- Hafeez HY, Lakhera SK, Karthik P, Anpo M, Neppolian B (2018) Facile construction of ternary CuFe<sub>2</sub>O<sub>4</sub>-TiO<sub>2</sub> nanocomposite supported reduced graphene oxide (rGO) photocatalysts for the efficient hydrogen production. *Appl Surf Sci* 449:772–779
- Hajjalilou E, Asgharzadeh H, Asl SK (2021) TiO<sub>2</sub>/rGO/Cu<sub>2</sub>O ternary hybrid for high-performance photoelectrochemical applications. *Appl Surf Sci* 544:148832
- He G, Ding J, Zhang J, Hao Q, Chen H (2015) One-step ball-milling preparation of highly photocatalytic active CoFe<sub>2</sub>O<sub>4</sub>-reduced graphene oxide heterojunctions for organic dye removal. *Ind Eng Chem Res* 54(11):2862–2867
- Hummers WS Jr, Offeman RE (1958) Preparation of graphitic oxide. *J Am Chem Soc* 80(6):1339–1339
- Iervolino G, Zammit I, Vaiano V, Rizzo L (2020) Limitations and prospects for wastewater treatment by UV and visible-light-active heterogeneous photocatalysis: a critical review. *Heterog Photocatal* 2020:225–264
- Ikram M, Raza A, Imran M, Ul-Hamid A, Shahbaz A, Ali S (2020) Hydrothermal synthesis of silver decorated reduced graphene oxide (rGO) nanoflakes with effective photocatalytic activity for wastewater treatment. *Nanoscale Res Lett* 15(1):1–11
- Ismail AA, Geioushy R, Bouzid H, Al-Sayari SA, Al-Hajry A, Bahne-mann DW (2013) TiO<sub>2</sub> decoration of graphene layers for highly efficient photocatalyst: impact of calcination at different gas atmosphere on photocatalytic efficiency. *Appl Catal B Environ* 129:62–70
- Jahanara K, Farhadi S (2019) A magnetically separable plate-like cadmium titanate–copper ferrite nanocomposite with enhanced visible-light photocatalytic degradation performance for organic contaminants. *RSC Adv* 9(27):15615–15628
- Jaramillo-Fierro X, Capa LF, Medina F, González S (2021) DFT study of methylene blue adsorption on ZnTiO<sub>3</sub> and TiO<sub>2</sub> surfaces (101). *Molecules* 26(13):3780
- Jiang G, Lin Z, Chen C, Zhu L, Chang Q, Wang N, Wei W, Tang H (2011) TiO<sub>2</sub> nanoparticles assembled on graphene oxide nanosheets with high photocatalytic activity for removal of pollutants. *Carbon* 49(8):2693–2701
- Jiang W-L, Ding Y-C, Haider MR, Han J-L, Liang B, Xia X, Yang L-M, Wang H-C, Peng Y-Z, Wang A-J (2020) A novel TiO<sub>2</sub>/graphite felt photoanode assisted electro-Fenton catalytic membrane process for sequential degradation of antibiotic florfenicol and elimination of its antibacterial activity. *Chem Eng J* 391:123503
- Kaur P, Frindy S, Park Y, Sillanpää M, Imteaz MA (2020) Synthesis of graphene-based biopolymer tio<sub>2</sub> electrodes using pyrolytic direct deposition method and its catalytic performance. *Catalysts* 10(9):1050
- Khan I, Saeed K, Zekker I, Zhang B, Hendi AH, Ahmad A, Ahmad S, Zada N, Ahmad H, Shah LA (2022) Review on methylene blue: its properties, uses, toxicity and photodegradation. *Water* 14(2):242
- Kim J, Park Y, Park H (2014) Solar hydrogen production coupled with the degradation of a dye pollutant using TiO<sub>2</sub> modified with platinum and nafion. *Int J Photoenergy* 2014:324859. <https://doi.org/10.1155/2014/324859>
- Kim G, Choi HJ, Kim H-I, Kim J, Monllor-Satoca D, Kim M, Park H (2016) Temperature-boostered photocatalytic H<sub>2</sub> production and charge transfer kinetics on TiO<sub>2</sub> under UV and visible light. *Photochem Photobiol Sci* 15(10):1247–1253
- Koca A, Şahin M (2002) Photocatalytic hydrogen production by direct sun light from sulfide/sulfite solution. *Int J Hydrog Energy* 27(4):363–367

- Kranz C, Wächtler M (2021) Characterizing photocatalysts for water splitting: from atoms to bulk and from slow to ultrafast processes. *Chem Soc Rev* 50(2):1407–1437
- Kumar P, Boukherroub R, Shankar K (2018) Sunlight-driven water-splitting using two-dimensional carbon based semiconductors. *J Mater Chem A* 6(27):12876–12931
- Kurniawan TA, Mengting Z, Fu D, Yeap SK, Othman MHD, Aytar R, Ouyang T (2020) Functionalizing TiO<sub>2</sub> with graphene oxide for enhancing photocatalytic degradation of methylene blue (MB) in contaminated wastewater. *J Environ Manag* 270:110871
- Li X, Yu J, Wageh S, Al-Ghamdi AA, Xie J (2016a) Graphene in photocatalysis: a review. *Small* 12(48):6640–6696
- Li Y, Tang Z, Zhang J, Zhang Z (2016b) Reduced graphene oxide three-dimensionally wrapped WO<sub>3</sub> hierarchical nanostructures as high-performance solar photocatalytic materials. *Appl Catal A Gen* 522:90–100
- Li T, Wang T, Qu G, Liang D, Hu S (2017) Synthesis and photocatalytic performance of reduced graphene oxide–TiO<sub>2</sub> nanocomposites for orange II degradation under UV light irradiation. *Environ Sci Pollut Res* 24(13):12416–12425
- Li F, Huang Y, Peng H, Cao Y, Niu Y (2020) Preparation and photocatalytic water splitting hydrogen production of titanium dioxide nanosheets. *Int J Photoenergy* 2020:3617312. <https://doi.org/10.1155/2020/3617312>
- Liang J, Wei Y, Zhang J, Yao Y, He G, Tang B, Chen H (2018) Scalable green method to fabricate magnetically separable NiFe<sub>2</sub>O<sub>4</sub>-reduced graphene oxide nanocomposites with enhanced photocatalytic performance driven by visible light. *Ind Eng Chem Res* 57(12):4311–4319
- Lim PF, Leong KH, Sim LC, Abd Aziz A, Saravanan P (2019) Amalgamation of N-graphene quantum dots with nanocubic like TiO<sub>2</sub>: an insight study of sunlight sensitive photocatalysis. *Environ Sci Pollut Res* 26(4):3455–3464
- Lin L-Y, Nie Y, Kavadiya S, Soundappan T, Biswas P (2017) N-doped reduced graphene oxide promoted nano TiO<sub>2</sub> as a bifunctional adsorbent/photocatalyst for CO<sub>2</sub> photoreduction: effect of N species. *Chem Eng J* 316:449–460
- Liu J, Wang Z, Liu L, Chen W (2011) Reduced graphene oxide as capturer of dyes and electrons during photocatalysis: surface wrapping and capture promoted efficiency. *Phys Chem Chem Phys* 13(29):13216–13221
- Liu W, Qian J, Wang K, Xu H, Jiang D, Liu Q, Yang X, Li H (2013) Magnetically separable Fe<sub>3</sub>O<sub>4</sub> nanoparticles-decorated reduced graphene oxide nanocomposite for catalytic wet hydrogen peroxide oxidation. *J Inorg Organomet Polym Mater* 23(4):907–916
- Liu G, Wang R, Liu H, Han K, Cui H, Ye H (2016) Highly dispersive nano-TiO<sub>2</sub> in situ growing on functional graphene with high photocatalytic activity. *J Nanopart Res* 18(1):21
- Liu X, Chen C, Chen XA, Qian G, Wang J, Wang C, Cao Z, Liu Q (2018) WO<sub>3</sub> QDs enhanced photocatalytic and electrochemical performance of GO/TiO<sub>2</sub> composite. *Catal Today* 315:155–161
- Liu WM, Li J, Zhang HY (2020) Reduced graphene oxide modified zinc oxide composites synergistic photocatalytic activity under visible light irradiation. *Optik* 207:163778
- Liu W, Tian Q, Yang J, Zhou Y, Chang H, Cui W, Xu Q (2021) A two-dimensional amorphous plasmonic heterostructure of Pd/MoO<sub>3</sub>-x for enhanced photoelectrochemical water splitting performance. *Chem—An Asian J* 16(10):1253–1257
- Long M, Qin Y, Chen C, Guo X, Tan B, Cai W (2013) Origin of visible light photoactivity of reduced graphene oxide/TiO<sub>2</sub> by in situ hydrothermal growth of undergrown TiO<sub>2</sub> with graphene oxide. *J Phys Chem C* 117(32):16734–16741
- Mahfoz W, Abdul Aziz M, Shaheen Shah S, Al-Betar AR (2020) Enhanced oxygen evolution via electrochemical water oxidation using conducting polymer and nanoparticle composites. *Chem—An Asian J* 15(24):4358–4367
- Meenakshisundaram S (2017) Environmental photocatalysis/photocatalytic decontamination. *Handbook of eco materials*. Springer, Cham, pp 1–16. <https://doi.org/10.1007/978-3-319-48281-1>
- Mino L, Zecchina A, Martra G, Rossi AM, Spoto G (2016) A surface science approach to TiO<sub>2</sub> P25 photocatalysis: an in situ FTIR study of phenol photodegradation at controlled water coverages from sub-monolayer to multilayer. *Appl Catal B Environ* 196:135–141
- Mohan VB, Lau K-T, Hui D, Bhattacharyya D (2018) Graphene-based materials and their composites: a review on production, applications and product limitations. *Compos Part B* 142:200–220
- Mondal A, Prabhakaran A, Gupta S, Subramanian VR (2021) Boosting photocatalytic activity using reduced graphene oxide (RGO)/semiconductor nanocomposites: issues and future scope. *ACS Omega* 6(13):8734–8743
- Morales-Torres S, Pastrana-Martínez LM, Figueiredo JL, Faria JL, Silva AM (2012) Design of graphene-based TiO<sub>2</sub> photocatalysts—a review. *Environ Sci Pollut Res* 19(9):3676–3687
- Moustafa HM, Obaid M, Nassar MM, Abdelkareem MA, Mahmoud MS (2020) Titanium dioxide-decorated rGO as an effective electrode for ultrahigh-performance capacitive deionization. *Sep Purif Technol* 235:116178
- Naldoni A, Altomare M, Zoppellaro G, Liu N, Kment Š, Zbořil R, Schmuki P (2019) Photocatalysis with reduced TiO<sub>2</sub>: from black TiO<sub>2</sub> to cocatalyst-free hydrogen production. *ACS Catal* 9(1):345–364
- Nayak S, Parida K (2020) Superactive NiFe-LDH/graphene nanocomposites as competent catalysts for water splitting reactions. *Inorg Chem Front* 7(20):3805–3836
- Nayak S, Parida K (2021) Recent progress in LDH@ graphene and analogous heterostructures for highly active and stable photocatalytic and photoelectrochemical water splitting. *Chem—An Asian J* 16(16):2211–2248
- Nazari Y, Salem S (2019) Efficient photocatalytic methylene blue degradation by Fe<sub>3</sub>O<sub>4</sub>@ TiO<sub>2</sub> core/shell linked to graphene by aminopropyltrimethoxysilane. *Environ Sci Pollut Res* 26(24):25359–25371
- Nguyen-Phan T-D, Pham VH, Yun H, Kim EJ, Hur SH, Chung JS, Shin EW (2011) Influence of heat treatment on thermally-reduced graphene oxide/TiO<sub>2</sub> composites for photocatalytic applications. *Korean J Chem Eng* 28(12):2236–2241
- Nowotny J, Sorrell C, Sheppard L, Bak T (2005) Solar-hydrogen: environmentally safe fuel for the future. *Int J Hydrog Energy* 30(5):521–544
- Park S, An J, Potts JR, Velamakanni A, Murali S, Ruoff RS (2011) Hydrazine-reduction of graphite-and graphene oxide. *Carbon* 49(9):3019–3023
- Pastrana-Martinez LM, Morales-Torres S, Likodimos V, Falaras P, Figueiredo JL, Faria JL, Silva AM (2014) Role of oxygen functionalities on the synthesis of photocatalytically active graphene–TiO<sub>2</sub> composites. *Appl Catal B Environ* 158:329–340
- Patil SS, Mali MG, Hassan MA, Patil DR, Kolekar SS, Ryu S-W (2017) One-pot in situ hydrothermal growth of BiVO<sub>4</sub>/Ag/rGO hybrid architectures for solar water splitting and environmental remediation. *Sci Rep* 7(1):1–12
- Pedrosa M, Pastrana-Martínez LM, Pereira MFR, Faria JL, Figueiredo JL, Silva AM (2018) N/S-doped graphene derivatives and TiO<sub>2</sub> for catalytic ozonation and photocatalysis of water pollutants. *Chem Eng J* 348:888–897
- Peiris S, de Silva HB, Ranasinghe KN, Bandara SV, Perera IR (2021) Recent development and future prospects of TiO<sub>2</sub> photocatalysis. *J Chin Chem Soc* 68(5):738–769
- Petala A, Noe A, Frontistis Z, Drivas C, Kennou S, Mantzavinos D, Kondarides DI (2019) Synthesis and characterization of CoOx/BiVO<sub>4</sub> photocatalysts for the degradation of propyl paraben. *J Hazard Mater* 372:52–60



- Prabhu S, Pudukudy M, Sohila S, Harish S, Navaneethan M, Navaneethan D, Ramesh R, Hayakawa Y (2018) Synthesis, structural and optical properties of ZnO spindle/reduced graphene oxide composites with enhanced photocatalytic activity under visible light irradiation. *Opt Mater* 79:186–195
- Pradhan GK, Padhi DK, Parida K (2013) Fabrication of  $\alpha$ -Fe<sub>2</sub>O<sub>3</sub> nanorod/RGO composite: a novel hybrid photocatalyst for phenol degradation. *ACS Appl Mater Interfaces* 5(18):9101–9110
- Purabgola A, Mayilswamy N, Kandasubramanian B (2022) "Graphene-based TiO<sub>2</sub> composites for photocatalysis & environmental remediation: synthesis and progress." *Environ Sci Pollut Res* 1-21
- Qi K, Xie Y, Wang R, Liu S-Y, Zhao Z (2019) Electroless plating Ni-P cocatalyst decorated g-C<sub>3</sub>N<sub>4</sub> with enhanced photocatalytic water splitting for H<sub>2</sub> generation. *Appl Surf Sci* 466:847–853
- Raghavulu Thirumalai DP, Løgstrup Andersen T, Markussen CM, Madsen B, Lilholt H (2013) Tensile and compression properties of hybrid composites – a comparative study. In Proceedings of the 19th international conference on composite materials (ICCM19) (pp 1029–1035). Canadian Association for Composite Structures and Materials
- Ramar V, Balasubramanian K (2019) Optical and highly enhanced solar light-driven photocatalytic activity of reduced graphene oxide wrapped  $\alpha$ -MoO<sub>3</sub> nanoplates. *Sol Energy* 194:1–10
- Ramar V, Balasubramanian K (2021) Reduced graphene oxide/WO<sub>3</sub> nanorod composites for photocatalytic degradation of methylene blue under sunlight irradiation. *ACS Appl Nano Mater* 4:5512–5521
- Ramar V, Moothattu S, Balasubramanian K (2018) Metal free, sunlight and white light based photocatalysis using carbon quantum dots from Citrus grandis: a green way to remove pollution. *Sol Energy* 169:120–127
- Ranjith KS, Manivel P, Rajendrakumar RT, Uyar T (2017) Multifunctional ZnO nanorod-reduced graphene oxide hybrids nanocomposites for effective water remediation: effective sunlight driven degradation of organic dyes and rapid heavy metal adsorption. *Chem Eng J* 325:588–600
- Rauf MA, Meetani MA, Khaleel A, Ahmed A (2010) Photocatalytic degradation of methylene blue using a mixed catalyst and product analysis by LC/MS. *Chem Eng J* 157(2-3):373–378
- Reddy NR, Bharagav U, Kumari MM, Cheralathan K, Shankar M, Reddy KR, Saleh TA, Aminabhavi TM (2020) Highly efficient solar light-driven photocatalytic hydrogen production over Cu/FCNTs-titania quantum dots-based heterostructures. *J Environ Manag* 254:109747
- Ribao P, Rivero MJ, Ortiz I (2017) TiO<sub>2</sub> structures doped with noble metals and/or graphene oxide to improve the photocatalytic degradation of dichloroacetic acid. *Environ Sci Pollut Res* 24(14):12628–12637
- Ruidíaz-Martínez M, Álvarez MA, López-Ramón MV, Cruz-Quesada G, Rivera-Utrilla J, Sánchez-Polo M (2020) Hydrothermal synthesis of rGO-TiO<sub>2</sub> composites as high-performance UV photocatalysts for ethylparaben degradation. *Catalysts* 10(5):520
- Safajou H, Ghanbari M, Amiri O, Khojasteh H, Namvar F, Zinatloo-Ajabshir S, Salavati-Niasari M (2021) Green synthesis and characterization of RGO/Cu nanocomposites as photocatalytic degradation of organic pollutants in waste-water. *Int J Hydrog Energy* 46(39):20534–20546
- Shah SS, Aziz MA, Mohamedkhair AK, Qasem MAA, Hakeem AS, Nazal MK, Yamani ZH (2019) Preparation and characterization of manganese oxide nanoparticles-coated Albizia procera derived carbon for electrochemical water oxidation. *J Mater Sci Mater Electron* 30(17):16087–16098
- Shang H, Chen L, Wang Y, Liu H (2018) Efficient photocatalytic degradation of methylene blue by using GO/hemin/TiO<sub>2</sub> nanocomposite under visible irradiation. *Micro & Nano Lett* 13(5):646–651
- Shen J, Yan B, Shi M, Ma H, Li N, Ye M (2011) One step hydrothermal synthesis of TiO<sub>2</sub>-reduced graphene oxide sheets. *J Mater Chem* 21(10):3415–3421
- Sher Shah MSA, Park AR, Zhang K, Park JH, Yoo PJ (2012) Green synthesis of biphasic TiO<sub>2</sub>-reduced graphene oxide nanocomposites with highly enhanced photocatalytic activity. *ACS Appl Mater Interfaces* 4(8):3893–3901
- Shih K-Y, Kuan Y-L, Wang E-R (2021) One-step microwave-assisted synthesis and visible-light photocatalytic activity enhancement of BiOBr/RGO nanocomposites for degradation of methylene blue. *Materials* 14(16):4577
- Singh R, Dutta S (2018) A review on H<sub>2</sub> production through photocatalytic reactions using TiO<sub>2</sub>/TiO<sub>2</sub>-assisted catalysts. *Fuel* 220:607–620
- Singh N, Jana S, Singh GP, Dey R (2020a) Graphene-supported TiO<sub>2</sub>: study of promotion of charge carrier in photocatalytic water splitting and methylene blue dye degradation. *Adv Compos Hybrid Mater* 3(1):127–140
- Singh P, Shandilya P, Raizada P, Sudhaik A, Rahmani-Sani A, Hosseini-Bandegharai A (2020b) Review on various strategies for enhancing photocatalytic activity of graphene based nanocomposites for water purification. *Arab J Chem* 13(1):3498–3520
- Siong VLE, Lee KM, Juan JC, Lai CW, Tai XH, Khe CS (2019) Removal of methylene blue dye by solvothermally reduced graphene oxide: a metal-free adsorption and photodegradation method. *RSC Adv* 9(64):37686–37695
- Soltani T, Tayyebi A, Lee B-K (2018) Efficient promotion of charge separation with reduced graphene oxide (rGO) in BiVO<sub>4</sub>/rGO photoanode for greatly enhanced photoelectrochemical water splitting. *Sol Energy Mater Sol Cells* 185:325–332
- Sonu K, Puttaiah SH, Raghavan VS, Gorthi SS (2021) Photocatalytic degradation of MB by TiO<sub>2</sub>: studies on recycle and reuse of photocatalyst and treated water for seed germination. *Environ Sci Pollut Res* 28(35):48742–48753
- Sultana S, Mansingh S, Parida K (2018) Facile synthesis of CeO<sub>2</sub> nanosheets decorated upon BiOI microplate: a surface oxygen vacancy promoted z-scheme-based 2D-2D nanocomposite photocatalyst with enhanced photocatalytic activity. *J Phys Chem C* 122(1):808–819
- Tang B, Chen H, Peng H, Wang Z, Huang W (2018) Graphene modified TiO<sub>2</sub> composite photocatalysts: mechanism, progress and perspective. *Nanomaterials* 8(2):105
- Tao W, Wang M, Ali R, Nie S, Zeng Q, Yang R, Lau W-M, He L, Tang H, Jian X (2019) Multi-layered porous hierarchical TiO<sub>2</sub>/g-C<sub>3</sub>N<sub>4</sub> hybrid coating for enhanced visible light photocatalysis. *Appl Surf Sci* 495:143435
- Teodosiu C, Fiore S (2019) Environmental and energy assessment of municipal wastewater treatment plants in Italy and Romania: a comparative study. *Water* 11(8):1611
- Timmerberg S, Kaltschmitt M, Finkbeiner M (2020) Hydrogen and hydrogen-derived fuels through methane decomposition of natural gas—GHG emissions and costs. *Energy Conv Manag*: X 7:100043
- Tran Thi VH, Cao TH, Pham TN, Pham TT, Le MC (2019) Synergistic adsorption and photocatalytic activity under visible irradiation using Ag-ZnO/GO nanoparticles derived at low temperature. *J Chem* 2019:2979517. <https://doi.org/10.1155/2019/2979517>
- Tran TTH, Kosslick H, Schulz A, Nguyen QL (2017) Photocatalytic performance of crystalline titania polymorphs in the degradation of hazardous pharmaceuticals and dyes. *Adv Nat Sci Nanosci Nanotechnol* 8(1):015011
- Ullah H, Loh A, Trudgeon DP, Li X (2020) Density functional theory study of NiFeCo ternary oxy-hydroxides for an efficient

- and stable oxygen evolution reaction catalyst. *ACS Omega* 5(32):20517–20524
- Usman M, Humayun M, Shah SS, Ullah H, Tahir AA, Khan A (2021) Bismuth-graphene nanohybrids: synthesis, reaction mechanisms, and photocatalytic applications—a review. *Energies* 14(8):2281
- Wang J-P, Yang H-C, Hsieh C-T (2012) Visible-light photodegradation of dye on co-doped titania nanotubes prepared by hydrothermal synthesis. *Int J Photoenergy* 2012:206534. <https://doi.org/10.1155/2012/206534>
- Wang M, Shen S, Li L, Tang Z, Yang J (2017) Effects of sacrificial reagents on photocatalytic hydrogen evolution over different photocatalysts. *J Mater Sci* 52(9):5155–5164
- Wang G, Long X, Qi K, Dang S, Zhong M, Xiao S, Zhou T (2019) Two-dimensional CdS/g-C<sub>6</sub>N<sub>6</sub> heterostructure used for visible light photocatalysis. *Appl Surf Sci* 471:162–167
- Wilke K, Breuer H (1999) The influence of transition metal doping on the physical and photocatalytic properties of titania. *J Photochem Photobiol A Chem* 121(1):49–53
- Wu Y, Chen X, Cao J, Zhu Y, Yuan W, Hu Z, Ao Z, Brudvig GW, Tian F, Yu JC, Li C (2022) Photocatalytically recovering hydrogen energy from wastewater treatment using MoS<sub>2</sub>@TiO<sub>2</sub> with sulfur/oxygen dual-defect. *Appl Catal B Environ* 303:120878
- Xu B, Yue S, Sui Z, Zhang X, Hou S, Cao G, Yang Y (2011) What is the choice for supercapacitors: graphene or graphene oxide? *Energy Environ Sci* 4(8):2826–2830
- Yan B, Chen Z, Xu Y (2020) Amorphous and crystalline 2D polymeric carbon nitride nanosheets for photocatalytic hydrogen/oxygen evolution and hydrogen peroxide production. *Chem—An Asian J* 15(15):2329–2340
- Yang HG, Sun CH, Qiao SZ, Zou J, Liu G, Smith SC, Cheng HM, Lu GQ (2008) Anatase TiO<sub>2</sub> single crystals with a large percentage of reactive facets. *Nature* 453(7195):638–641
- Yang B, Tian Z, Zhang L, Guo Y, Yan S (2015a) Enhanced heterogeneous Fenton degradation of methylene blue by nanoscale zero valent iron (nZVI) assembled on magnetic Fe<sub>3</sub>O<sub>4</sub>/reduced graphene oxide. *J Water Process Eng* 5:101–111
- Yang X, Chen W, Huang J, Zhou Y, Zhu Y, Li C (2015b) Rapid degradation of methylene blue in a novel heterogeneous Fe<sub>3</sub>O<sub>4</sub>@rGO@TiO<sub>2</sub>-catalyzed photo-Fenton system. *Sci Rep* 5(1):1–10
- Yang G, Li L, Lee WB, Ng MC (2018) Structure of graphene and its disorders: a review. *Sci Technol Adv Mater* 19(1):613–648
- Yaqoob L, Noor T, Iqbal N, Nasir H, Sohail M, Zaman N, Usman M (2020) Nanocomposites of cobalt benzene tricarboxylic acid MOF with rGO: an efficient and robust electrocatalyst for oxygen evolution reaction (OER). *Renew Energy* 156:1040–1054
- Yu H-F (2007) Phase development and photocatalytic ability of gel-derived P-doped TiO<sub>2</sub>. *J Mater Res* 22(9):2565–2572
- Yu G, Lu Y, Guo J, Patel M, Bafana A, Wang X, Qiu B, Jeffries C, Wei S, Guo Z (2018) Carbon nanotubes, graphene, and their derivatives for heavy metal removal. *Adv Compos Hybrid Mater* 1(1):56–78
- Yu W, Sisi L, Haiyan Y, Jie L (2020) Progress in the functional modification of graphene/graphene oxide: a review. *RSC Adv* 10(26):15328–15345
- Zhang Y, Tang Z-R, Fu X, Xu Y-J (2010) TiO<sub>2</sub>-graphene nanocomposites for gas-phase photocatalytic degradation of volatile aromatic pollutant: is TiO<sub>2</sub>-graphene truly different from other TiO<sub>2</sub>-carbon composite materials? *ACS Nano* 4(12):7303–7314
- Zhang W, Li Y, Wang C, Wang P, Wang Q, Wang D (2013) Mechanisms of simultaneous hydrogen production and estrogenic activity removal from secondary effluent through solar photocatalysis. *Water Res* 47(9):3173–3182
- Zhang G, Zhang W, Crittenden J, Minakata D, Chen Y, Wang P (2014) Effects of inorganic electron donors in photocatalytic hydrogen production over Ru/(CuAg)<sub>0.15</sub>In<sub>0.3</sub>Zn<sub>1.4</sub>S<sub>2</sub> under visible light irradiation. *J Renew Sustain Energy* 6(3):033131
- Zhang Y, Zhang Y, Li X, Zhao X, Anning C, Crittenden J, Lyu X (2020) Photocatalytic water splitting of ternary graphene-like photocatalyst for the photocatalytic hydrogen production. *Front Environ Sci Eng* 14:69
- Zhao X, Zhang G, Zhang Z (2020) TiO<sub>2</sub>-based catalysts for photocatalytic reduction of aqueous oxyanions: state-of-the-art and future prospects. *Environ Int* 136:105453

**Publisher's note** Springer Nature remains neutral with regard to jurisdictional claims in published maps and institutional affiliations.

Springer Nature or its licensor holds exclusive rights to this article under a publishing agreement with the author(s) or other rightsholder(s); author self-archiving of the accepted manuscript version of this article is solely governed by the terms of such publishing agreement and applicable law.